Relativistic Structural Characterization of Molybdenum and Tungsten Disulfide Materials

Micheal Arockiaraj[a], **Sandi Klavžar**[b,c,d], **S. Ruth Julie Kavitha**[a]*,
Shagufa Mushtaq[e] , **Krishnan Balasubramanian**[f]

[a]Department of Mathematics, Loyola College, Chennai 600034, India

[b]Faculty of Mathematics and Physics, University of Ljubljana, Slovenia

[c]Faculty of Natural Sciences and Mathematics, University of Maribor, Slovenia

[d]Institute of Mathematics, Physics and Mechanics, Ljubljana, Slovenia

[e]Department of Mathematics, Loyola College, University of Madras, Chennai 600034, India

[f]School of Molecular Sciences, Arizona State University, Tempe AZ 85287-1604, USA

Abstract

The advent of two-dimensional transition metal dichalcogenides has triggered an interest in exploring a new class of high performance materials with intriguing physico-chemical attributes. Molybdenum and tungsten disulfides have attracted significant attention due to surface excitons and trions, and large spin-orbit effects in these compounds. Moreover, WS_2 is especially intriguing due to large relativistic effects which result in bound excitons at the edge and biexciton formation in the bilayers. Hence we present a relativistic topological model for the characterization of these two types of metal disulfides. We have employed relativistically weighted graph-theoretical methods for obtaining structural descriptors of these compounds by inclusion of different shapes on the boundaries and employing the topological cut techniques.

Keywords: Relativistic topological indices; cut method; monolayers; distance-based descriptors.

1 Introduction

A new class of two-dimensional monolayer materials has received considerable interest in recent years ever since the advent of 2D graphene materials with novel properties. However, most of the available 2D materials in the pristine forms are intrinsically nonmagnetic and this thus limits their range of

*Corresponding author : juliesuresh91@gmail.com

applications. Hence it is desirable to explore such novel 2D materials with a robust intrinsic ferromagnetic order for optimizing the device applications. Subsequently, the transition metal dichalcogenides (TMDs) [1] have been identified as notable candidates for their exclusive ferromagnetism, optical properties, surface excitonic features, and their ability to intercalate and exfoliate have all contributed to a wide range of applications. Consequently, these materials find applications in a number of areas such as spintronics, energy harvesting, DNA sequencing, and personalized medicine as they possess a unique combination of atomic-scale thickness, spin-orbit coupling, direct bandgap, and other favorable electronic and mechanical properties [2]. Tungsten disulfide in its 2D form exhibits strongly bound excitons even at the edge, trion fine structures, and interesting spin dynamics attributed to a large spin-orbit splitting of the tungsten atoms, all of which result in unusual optical properties of WS_2 [3].

Recent advances in sample preparation, optical detection, transfer and manipulation of 2D materials have also triggered a resurgence of scientific and engineering interest in TMDs. In particular, the monolayers of two-dimensional crystals are emphasized more in industrial aspects than their bulk structure as the reduced dimensions significantly enhance many physical characteristics [2]. For instance, the indirect bandgap of 1.3 eV in the bulk phase of MoS_2 changes to a direct bandgap of 1.8 eV in the single-layer form [4] thus opening the possibility of a wide range of optoelectronic applications [5]. As there exist many such interesting layer-dependent properties in 2D materials that differ significantly from the properties of the bulk materials, the investigation of various methods to scale the monolayers from their bulk phase has gained its momentum in recent years [2, 6].

The transition metal disulfides MS_2 (M = Mo,W) are popular among the TMDs that exhibit ideal magnetic and electrical characteristics for exploring the valley-based optoelectronic applications [7, 8]. Their strong in-plane bonding and weak out-of-plane interactions enable the exfoliation of two-dimensional layers of single unit cell thickness although in the case of WS_2 exfoliation is more difficult due to stronger binding between the layers caused by both scalar relativistic effects such as mass-velocity effects, Darwin correction and spinor based spin-orbit effects [9, 10], especially for tungsten. Even the ground electronic state of tungsten is altered by relativistic effects as shown by a previous study [10]. The attainment of a single layer with atomic thickness [6] has enhanced their technological importance as the monolayers exhibit exceptional attributes including amplification of electrical signals with less power consumption, ultralow standby power dissipation, and high mobility rates. The direct bandgap, the electronic structure of their monolayers, and the propensity to form WS_2 nanotubes emphasize their key roles in various fields such as the lithium ion batteries (LIB) [11], flexible electronic devices [12], photovoltaics [13], and valleytronics [14]. Furthermore, their abundant availability helps in achieving cost-effective thermoelectric devices when compared to other conventional materials like bismuth telluride, offering a unique opportunity of realizing flexile generators

for the wearable technology. Recently Manzeli et al. [15] summarized the various methods used to synthesize these TMDs and their intriguing properties with particular attention to their topological phases.

It is to be observed that the physical properties of the newly synthesized 2D materials are extremely sensitive to various thermodynamic and kinetic conditions of the growth process [16], leading to numerous expensive trial and error experiments. These challenges were addressed by the development of various theoretical and computational methods in modeling these materials, which is effective in understanding the conditions of the growth mechanism. The recent survey [17] and the computational study [18] provide an outlook of various computational and theoretical approaches to 2D materials synthesis and growth in general. In particular, it has been also pointed out that bond-additive indices could be employed for the determination of peripheral shape correlations of a chemical compound [19]. Henceforth, relativistic quantum computations could be used as potential tools in determining their physical attributes and performance characterization through relativistic quantum electrostatic potentials.

Graph theory provides powerful and efficient tools for the topological characterization of the underlying structural features through the connectivity of the network. Any problem that involves a graph structure can be analyzed and solved using graph-theoretical tools which in turn expand the scope of utilization in numerous areas of science and engineering. In particular, chemical graph theory deals with the characterization of the underlying topology by providing elegant structural descriptors called the topological indices that have the efficacy to correlate with the observed properties. It is largely applied to attain the quantitative characterization of material structures, thereby enabling the study of quantitative structure-activity (QSAR), property (QSPR), and toxicity (QSTR) relationships of the 2D molecular structures [20].

Topological indices are invariant to the labeling of vertices, and thus form a reliable starting point in the quantitative study of molecules and in assisting data set reduction thereby reducing the final candidates for computationally intensive quantum chemical techniques. These nonemperic numerical quantities can be significantly utilized due to their cost-effectiveness and computational efficiency of their graph-theoretic techniques in readily determining and predicting the characteristics of such complex structures, thus providing powerful alternatives to analyze and experiment the chemical compounds. In the past decades, numerous papers were devoted to the study of such topological descriptors owing to its ability to predict the pharmacological and physico-chemical attributes of a compound theoretically [21]. Moreover, such mathematical classifications including hypercubes can have far-reaching applications in chemistry including explorations into quantum similarity measures of the periodic table of elements and periodicity of aromatic compounds [22].

Topological indices such as Szeged index, Gutman index, Mostar index and their variants are extremely useful in characterizing topostructural and peripheral properties of materials [23–28]. The above mentioned topological indices can be computed in an elegant way by locating appropriate edge cuts provided the given chemical material belongs to the family of partial cubes. But in the development of such techniques for a 2D complex molecular structure has been quite challenging due to computational complexities in the implementation process. In the current study, we have developed novel contraction procedures to facilitate the computation of topological indices for 2D materials such as MoS_2 and WS_2. Moreover, we have incorporated relativistic effects in our topological models for realistic predictions on WS_2.

Although a graph theoretical model only depicts the underlying topology of the materials and not the chemical or quantum features, a very little progress (see [29]) has been made to integrate topological descriptors to the chemistry specific features such as electronic features, and especially for materials containing very heavy atoms. Recently a relativistic topological model was proposed [30] by incorporating relativistic quantum chemical structural parameters through weights assigned to each vertex and edge of the 2D network. In the current study, we employ the relativistic structural descriptors to characterizing 2D transition metal disulfides through relativistically strength-weighted graphs.

2 Mathematical Preliminaries

A simple connected graph G comprises of a vertex set $V(G)$ and an edge set $E(G)$. For any two vertices $u, v \in V(G)$, the distance $d_G(u, v)$ between them is defined as the number of edges on a shortest path connecting them. Similarly, we define the distance between a vertex u and an edge $f = ab$ as $d_G(u, f) = \min\{d_G(u, a), d_G(u, b)\}$ and the distance between two edges $e = uv$ and $f = ab$ as $D_G(f, g) = \min\{d_G(e, a), d_G(e, b)\}$.

The degree $d_G(u)$ of a vertex u is the number of edges incident to the vertex u and and the degree $d_G(e)$ of an edge e is defined as the number of edges adjacent to e. In view of the degrees of end vertices of the edge, the weighted bond measures of $e = uv$ with respect to sum and product are defined as $w_e^+(e) = d_G(u) + d_G(v)$ and $w_e^*(e) = d_G(u)d_G(v)$ respectively.

The neighborhood $N_G(v)$ of a vertex v is the set of all vertices adjacent to the vertex v and the closeness sets of an edge $e = uv \in E(G)$ are defined as follows:

$$\begin{aligned} N_u(e|G) &= \{x \in V(G) : \ d_G(u, x) < d_G(v, x)\}, \\ M_u(e|G) &= \{f \in E(G) : \ d_G(u, f) < d_G(v, f)\}. \end{aligned}$$

Table 1: Topological indices of G_{sw} where $e = uv$

Variants	Mathematical Expressions
Wiener	$W(G_{sw}) = \sum_{\{u,v\}\subseteq V(G_{sw})} w_v(u)w_v(v)d_{G_{sw}}(u,v)$ $W_e(G_{sw}) = \sum_{\{u,v\}\subseteq V(G_{sw})} s_v(u)\ s_v(v)\ d_{G_{sw}}(u,v)\ + \sum_{\{e,f\}\subseteq E(G_{sw})} s_e(e)\ s_e(f)\ D_{G_{sw}}(e,f) + \sum_{u\in V(G_{sw})}\sum_{f\in E(G_{sw})} s_v(u)\ s_e(f)\ d_{G_{sw}}(u,f)$ $W_{ev}(G_{sw}) = \frac{1}{2}\Big(\sum_{\{u,v\}\subseteq V(G_{sw})} \{w_v(u)\ s_v(v)\ +\ w_v(v)\ s_v(u)\}\ d_{G_{sw}}(u,v) + \sum_{u\in V(G_{sw})}\sum_{f\in E(G_{sw})} w_v(u)\ s_e(f)\ d_{G_{sw}}(u,f)\Big)$
Szeged	$Sz_v(G_{sw}) = \sum_{e\in E(G_{sw})} s_e(e)n_u(e\|G_{sw})n_v(e\|G_{sw})$ $Sz_e(G_{sw}) = \sum_{e\in E(G_{sw})} s_e(e)m_u(e\|G_{sw})m_v(e\|G_{sw})$ $Sz_{ev}(G_{sw}) = \frac{1}{2}\sum_{e\in E(G_{sw})} s_e(e)\Big[n_u(e\|G_{sw})m_v(e\|G_{sw}) + n_v(e\|G_{sw})m_u(e\|G_{sw})\Big]$ $Sz_t(G_{sw}) = Sz_v(G_{sw}) + Sz_e(G_{sw}) + 2Sz_{ev}(G_{sw})$
Padmakar-Ivan	$PI(G_{sw}) = \sum_{e\in E(G_{sw})} s_e(e)\Big[m_u(e\|G_{sw}) + m_v(e\|G_{sw})\Big]$
Mostar	$Mo(G_{sw}) = \sum_{e\in E(G_{sw})} s_e(e)\|n_u(e\|G_{sw}) - n_v(e\|G_{sw})\|$ $w^+Mo(G_{sw}) = \sum_{e\in E(G_{sw})} w_e^+(e)\|n_u(e\|G_{sw}) - n_v(e\|G_{sw})\|$ $w^*Mo(G_{sw}) = \sum_{e\in E(G_{sw})} w_e^*(e)\|n_u(e\|G_{sw}) - n_v(e\|G_{sw})\|$
Edge-Mostar	$Mo_e(G_{sw}) = \sum_{e\in E(G_{sw})} s_e(e)\|m_u(e\|G_{sw}) - m_v(e\|G_{sw})\|$ $w^+Mo_e(G_{sw}) = \sum_{e\in E(G_{sw})} w_e^+(e)\|m_u(e\|G_{sw}) - m_v(e\|G_{sw})\|$ $w^*Mo_e(G_{sw}) = \sum_{e\in E(G_{sw})} w_e^*(e)\|m_u(e\|G_{sw}) - m_v(e\|G_{sw})\|$
Total-Mostar	$Mo_t(G_{sw}) = \sum_{e\in E(G_{sw})} s_e(e)\|t_u(e\|G_{sw}) - t_v(e\|G_{sw})\|$ $w^+Mo_t(G_{sw}) = \sum_{e\in E(G_{sw})} w_e^+(e)\|t_u(e\|G_{sw}) - t_v(e\|G_{sw})\|$ $w^*Mo_t(G_{sw}) = \sum_{e\in E(G_{sw})} w_e^*(e)\|t_u(e\|G_{sw}) - t_v(e\|G_{sw})\|$
Schultz	$S(G_{sw}) = \sum_{\{u,v\}\subseteq V(G_{sw})} \Big[w_v(v)[d_{G_{sw}}(u) + 2s_v(u)] + w_v(u)[d_{G_{sw}}(v) + 2s_v(v)]\Big] d_{G_{sw}}(u,v)$
Gutman	$Gut(G_{sw}) = \sum_{\{u,v\}\subseteq V(G_{sw})} [d_{G_{sw}}(u) + 2s_v(u)][d_{G_{sw}}(v) + 2s_v(v)]d_{G_{sw}}(u,v)$

The counts of the sets $N_u(e|G)$ and $M_u(e|G)$ are denoted as $n_u(e|G)$ and $m_u(e|G)$, respectively, and $t_u(e|G)$ denotes their sum. The values of $n_v(e|G)$, $m_v(e|G)$ and $t_v(e|G)$ are analogous.

For $K \subseteq E(G)$, the vertex set of a quotient graph G/K consists of the connected components of the graph $G - K$, and two components C and D being adjacent if there exists an edge $cd \in K$ such that $c \in C$ and $d \in D$. A subgraph H of a graph G is said to be convex if for any two vertices $u, v \in H$, any shortest path between them in G lies completely in H, whereas H is an isometric subgraph if for every pair of vertices, the distance between them in both G and H are equal. An isometric subgraph of a hypercube is called a partial cube, where the hypercube Q_n of dimension n is defined as the Cartesian product of n copies of the complete graph K_2.

A strength-weighted graph [25] $G_{sw} = (G, SW_V, SW_E)$ is a graph G in which the vertex and edge set are assigned a pair of strength-weighted functions (SW_V, SW_E) defined as follows:

(i) $SW_V = (w_v, s_v)$, where $w_v, s_v : V(G_{sw}) \to \mathbb{R}_0^+$ are vertex-weight and strength functions,

(ii) $SW_E = (w_e, s_e)$, where $w_e, s_e : E(G_{sw}) \to \mathbb{R}_0^+$ are edge-weight and strength functions.

The structural terminologies such as distance, neighborhood and the closeness sets in G_{sw} remains the same as that of the simple graph G, whereas the degree and the cardinality of closeness sets in G_{sw} are defined in the following.

$$d_{G_{sw}}(u) = \sum_{x \in N_{G_{sw}}(u)} s_e(ux),$$

$$n_u(e|G_{sw}) = \sum_{x \in N_u(e|G_{sw})} w_v(x),$$

$$m_u(e|G_{sw}) = \sum_{x \in N_u(e|G_{sw})} s_v(x) + \sum_{f \in M_u(e|G_{sw})} s_e(f).$$

The formulae of several topological indices (TI) of a strength-weighted graph G_{sw} that are analyzed in this study are tabulated in Table 1, where $TI(G_{sw}) = TI(G)$ if $w_v = 1$, $s_v = 0$, $w_e = 1$ and $s_e = 1$. The computational techniques for evaluating these indices continues to be an interesting topic of research [23–25, 31] because it facilitates the topological characterization without actually calculating the numerical parameters of the graph. The cut method is a classical computational procedure [31] employed to investigate topological indices and is being revamped till date based on the kind of graphs [23, 25–27]. In this method, the key role is played by the Djoković-Winkler relation Θ, cf. [31]. This relation is defined on the edge set of a given graph G, where edges $e = uv$ and $f = ab$ of G are in relation Θ if $d_G(v, b) + d_G(u, a) \neq d_G(u, b) + d_G(v, a)$.

The relation Θ is reflexive and symmetric in general, but need not be transitive. In the bipartite case, Θ is transitive precisely on partial cubes. In general, the transitive closure Θ^* forms an equivalence relation, and thus partitions $E(G)$ into Θ^*-classes $F_1, \ldots, F_k$, whcih are called cuts. These cuts

dissect the given graph into two or more connected convex components in order to determine the corresponding descriptor of the compound [25–27,31]. A coarser partition Θ^{c*} is a partition $\{E_1, \ldots, E_p\}$ in which each set E_i is the union of one or more Θ^*-classes of G. The formulae for determining the topological indices using this technique is summarized in the following theorem.

Theorem 1. *[23–25] Let $G_{sw} = \big(G, (w_v, s_v), (w_e, s_e)\big)$ be a strength-weighted graph. Let $\mathcal{E}(G) = \{E_1, E_2, ..., E_p\}$ be a Θ^{c*}-partition of $E(G)$, and $TI \in \{W, W_e, W_{ev}, Sz_v, Sz_e, Sz_{ev}, PI, S, Gut, Mo, Mo_e, Mo_t, w^+Mo, w^+Mo_e, w^+Mo_t, w^*Mo, w^*Mo_e, w^*Mo_t\}$. Then,*

$$TI(G_{sw}) = \sum_{i=1}^{p} TI(G/E_i, (w_v^i, s_v^i), (w_e^i, s_e^i)),$$

where

(i) $w_v^i : V(G_{sw}/E_i) \to \mathbb{R}_0^+$, $w_v^i(X) = \sum\limits_{x \in V(X)} w_v(x)$, $\forall\ X \in V(G_{sw}/E_i)$,

(ii) $s_v^i : V(G_{sw}/E_i) \to \mathbb{R}_0^+$, $s_v^i(X) = \sum\limits_{xy \in E(X)} s_e(xy) \ + \sum\limits_{x \in V(X)} s_v(x)$, $\forall\ X \in V(G_{sw}/E_i)$,

(iii) $w_e^i : E(G_{sw}/E_i) \to \mathbb{R}_0^+$, $w_e^i(XY) = \sum\limits_{\substack{xy \in E_i \\ x \in V(X),\ y \in V(Y)}} w_e(xy), \forall\ XY \in E(G_{sw}/E_i)$,

where we apply

- *if $TI \in \{w^+Mo, w^+Mo_e, w^+Mo_t\}$, $w_e^i(XY) = w_e^{+i}(XY) = \sum\limits_{\substack{xy \in E_i \\ x \in V(X), y \in V(Y)}} (d_{G_{sw}}(x) + d_{G_{sw}}(y))$, $\forall\ XY \in E(G_{sw}/E_i)$,*
- *if $TI \in \{w^*Mo, w^*Mo_e, w^*Mo_t\}$, $w_e^i(XY) = w_e^{*i}(XY) = \sum\limits_{\substack{xy \in E_i \\ x \in V(X),\ y \in V(Y)}} d_{G_{sw}}(x) d_{G_{sw}}(y)$, $\forall\ XY \in E(G_{sw}/E_i)$.*
- *if TI is other than the above indices, w_e^i is not needed.*

(iv) $s_e^i : E(G_{sw}/E_i) \to \mathbb{R}_0^+$, $s_e^i(XY) = \sum\limits_{\substack{xy \in E_i \\ x \in V(X),\ y \in V(Y)}} s_e(xy), \forall\ XY \in E(G_{sw}/E_i)$.

3 Molybdenum and Tungsten Disulfides

As we noted in the introduction, molybdenum and tungsten disulfides are novel quasi-two-dimensional transition metal disulfides with excellent physico-chemical properties complementary to those of semimetallic graphene [32], promising several potential applications [7]. These are layered semiconductor materials of the form S–M–S, in which each plane of the metal (M) atoms are sandwiched between two layers of sulfur (S) atoms. Here the bonding within each sandwich layer is strongly covalent while

the individual S–M–S layers are loosely held through van der Waals interaction, which thus facilitates the exfoliation of a single layer to a few layers from the bulk [6]. The two popular crystal phases for the bulk MoS_2 and WS_2 structures are: (i) a thermodynamically stable 2H phase (hexagonal symmetry) with the $P63/mmc$ space group [33] (ii) a metastable 1T phase (trigonal symmetry) with the $P\bar{3}m1$ space group which are characterized by trigonal prismatic and octahedral coordination of metal atoms, respectively as shown in Figure 1. As these phases of MS_2 monolayers exhibit substantially different electronic properties (for example, 2H MoS_2 is a semiconductor whereas 1T MoS_2 is metallic [34]), the characterization of the structure in these phases is efficacious.

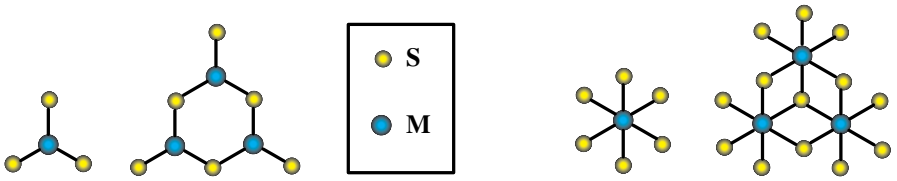

Figure 1: Unit cells and monolayers of MS_2 in (a) 2H phase (b) 1T phase

We apply relativistic topological models for the characterization of MoS_2 and WS_2 as relativistic effects including spin-orbit coupling are significant for such heavy transition metal atoms and main group atoms as Mo, W, Sn, Pd and so on [9,10,35]. Both scalar relativistic effects such as mass-velocity and Darwin corrections as well as 2-component spinor based spin-orbit coupling are quite significant. As shown in ref [10], even the ground state of tungsten atom is completely altered by spin-orbit effects compared to Cr and Mo which tend to have $(n-1)d^5ns^1$ ground states while W exhibits a $5d^46s^2$ ground state with a large spin-orbit splitting of over 6200 cm^{-1} or 0.77 eV [10]. These large spin-orbit effects manifest themselves in the optical, trion, excitonic properties and spin valley dynamics of WS_2, all of which are attributed to the large spin-orbit splitting of W. Spin-orbit effects not only influence the geometries of the molecules and materials containing heavy atoms but also completely alter the topological structures of potential energy surfaces [36, 37]. That is, the spin-orbit coupling is so large that it overtakes Jahn-Teller distortions and thus modifying the potential energy surfaces of such molecules [37]. This arises from the fact the overall symmetry of the molecule or material under consideration alters when spin-orbit coupling is included from the usual point group to the double group [9, 37] thereby allowing for mixing of two electronic states that would otherwise not mix. Such singlet-triplet mixings of electronic states caused by spin-orbit coupling result in very interesting topological spintronics in such heavy materials as WS_2. Thus it is of paramount importance to have topological models that include relativistic effects for realistic structural characterization of 2D WS_2 materials.

Relativistic parameters for the 2D materials under consideration can be obtained through a localization of relativistically obtained Bloch orbitals into Wannier functions by localized transformations such as the efficient Pipek-Mezey transformation [38]. Such computations need to include spin-orbit coupling which changes the Hamiltonian and thus allowing for the mixing of two states of different spin multiplicities and spatial symmetries that would otherwise not mix in the absence of spin-orbit coupling. For example, the mixing of singlet and triplet states caused by spin-orbit coupling would completely alter the Bloch orbitals and thus the Wannier functions of these materials. Consequently, one needs to adapt a two-component spinor description for systems such as WS_2 because of the large spin-orbit effects on the tungsten. The two-component Wannier spinors then provide a localized description of these materials. Once the localization procedure is accomplished through the Pipek-Mezey transform, one can obtain relativistic weights γ_M for the metal atom, γ_S for the sulfur atom and ρ_{MS} for each edge M–S in the 2D network of MoS_2 and WS_2. The relativistic weights thus obtained can then be transferred to structural attributes of two phases of MS_2 (M = Mo, W) by analyzing their molecular model in various forms depending on the arrangement of the corresponding unit cells [39,40].

3.1 Mathematical Key Idea

The key idea of this paper is to correctly locate the Θ-classes of 2H MS_2 and 1T MS_2 monolayers from their underlying graph structures. That is, we are going to show that the graph structures of 2H MS_2 and 1T MS_2 monolayers belong to the family of partial cubes.

The graph structure of 2H MS_2 monolayer can be easily constructed from benzenoid systems by attaching pendant edges in specific places on the boundaries as shown in Figure 2. That benzenoid systems are partial cubes is known already for a long time, cf. [31]. Moreover, it is clear (and well-known) that attaching pendant edges to partial cubes yields partial cubes again. Hence we can conclude that the graph structure of 2H MS_2 monolayers are partial cubes. The graph structure of 1T MS_2 monolayers can be constructed from 2H MS_2 graph structure by adding vertices and edges as shown in the right-hand side of Figure 2. To prove that 1T MS_2 graph structures are partial cubes, we need some preparation. Let G be a graph and let $W_1, W_2 \subseteq V(G)$ be vertex subsets that cover $V(G)$ and have nonempty intersection, that is, $W_1 \cup W_2 = V(G)$ and $W_1 \cap W_2 \neq \emptyset$. Assume further that the subgraphs induced by W_1 and by W_2 are isometric in G, as well as that there are no edges between $W_1 \setminus W_2$ and $W_2 \setminus W_1$. Under these assumptions, let H be a graph constructed as follows.

- Replace each vertex $w \in W_1 \cap W_2$ by vertices w_1 and w_2 and add the edge w_1w_2.
- Join w_1 and w_2 to all neighbors of w in $W_1 \setminus W_2$ and $W_2 \setminus W_1$, respectively.
- If $w, z \in W_1 \cap W_2$ and $wz \in E(G)$, then add edges w_1z_1 and w_2z_2.

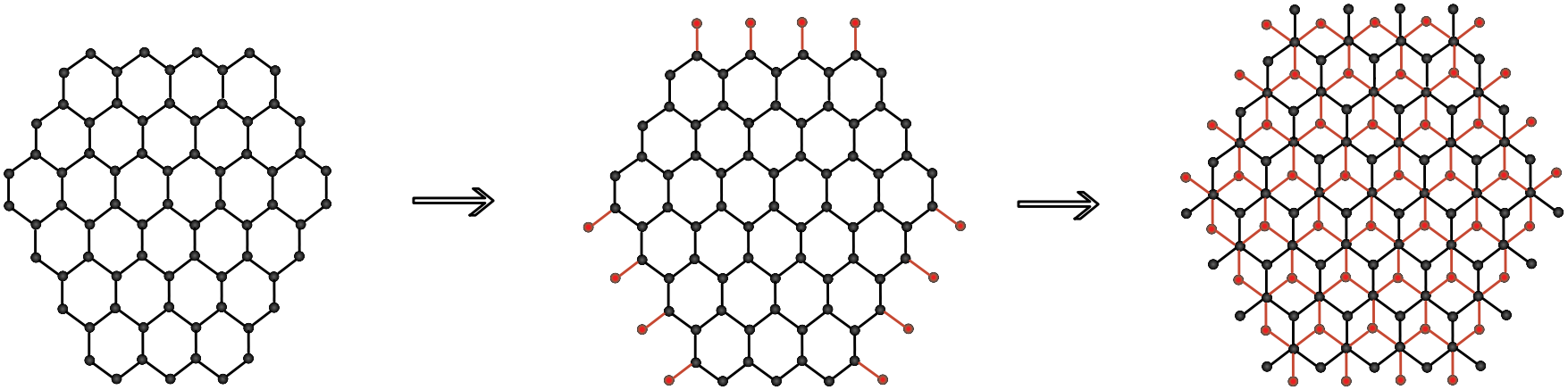

Figure 2: Construction of MoS_2 monolayers from benzenoid systems

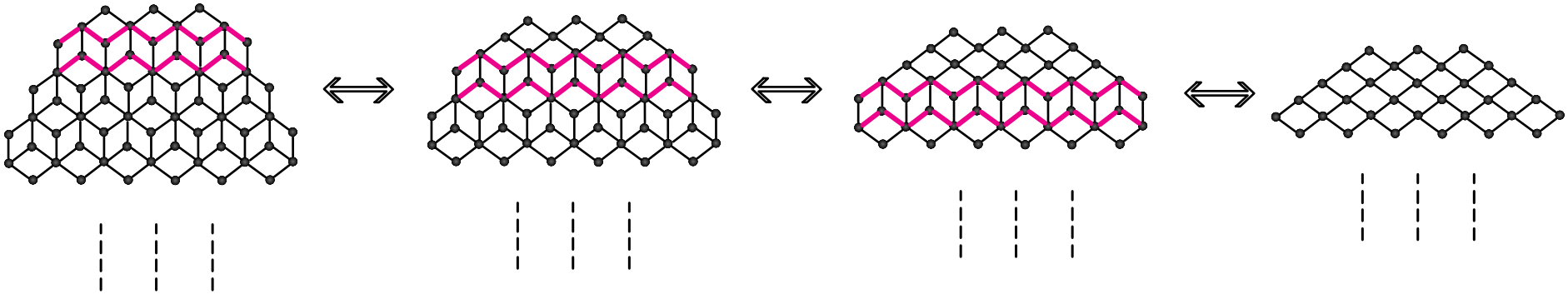

Figure 3: Various stages of 1T MS_2 monolayer by contraction procedure

Then we say that H is an *expansion of G with respect to W_1, W_2*. In addition, a *contraction* is the inverse operation of the expansion, that is, we say that in the above construction G is a *contraction of H*. Finally, an *expansion procedure* is a sequence of expansions. With this preparation we can now state the following characterization of partial cubes due to Chepoi [41].

Theorem 2. *A graph G is a partial cube if and only if G can be obtained from the one vertex graph K_1 by a sequence of expansions.*

Using Theorem 2 we can now deduce the following.

Theorem 3. *The graph structures of 1T MS_2 monolayers are partial cubes.*

Proof. It is enough to prove that the graph structure of 1T MS_2 without pendant edges are partial cubes. We now construct the 1T MS_2 monolayers without pendant edges as shown in Figure 3. First contract the "ladder" subgraph as shown in the Figure 3. Note that the bottom marked path is isometric in the graph, as well as it is the upper marked path, hence by Theorem 2, the left top graph is a partial cube if and only if the top right graph is a partial cube.

We then proceed analogously by contracting horizontal isometric paths from top to bottom. See Figure 3 again, where the next two steps of the contraction are presented. Continuing in this manner we end up with a grid-like graph H. By the same method (but simpler) we see that H is a partial cube. More precisely, we contract diagonal ladder subgraphs from, say, top left till bottom right. We conclude that since H is a partial cube, then so it is the starting 1T MS_2 monolayer. □

3.2 2H and 1T MS_2 monolayers

In the 2H phase, each metal atom M is prismatically coordinated by three surrounding sulfur atoms S, with the S atoms in the upper layer lying directly above those of the lower layer. The grain boundaries of these 2H monolayer MS_2 possess significant impact in the electronic, magnetic and transport properties of the compounds [20, 42].

In 1T MS_2 monolayers, the metal atom M is co-ordinated to six adjoining S atoms octahedrally, with the two S layers being stacked in the A–B packing mode. It is also claimed to exhibit several interesting properties such as strong adsorption of functional groups [39], extraordinary hydrogen evolution reaction (HER) catalytic activity [43] and so on. The schematic representation of the two types of MS_2 monolayers in the given two phases [39, 40] are depicted in Figures 4 and 5. The bitrapezium, hexagonal and parallelogram shapes of MS_2 monolayers are respectively denoted by $BT_j(n, p, q)$, $H_j(k) = BT_j(2k-1, k-1, k-1)$, and $P_j(p, q)$, where $j = \{H, T\}$ denotes their two different phases.

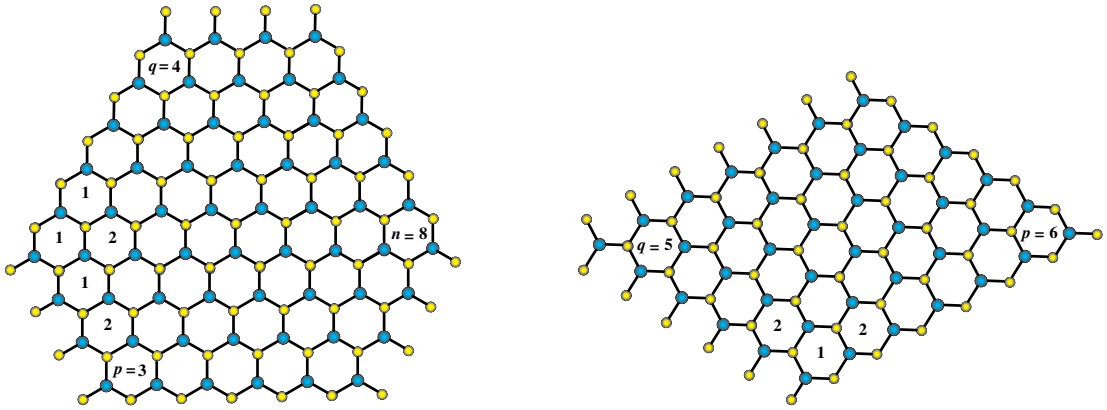

(a) (b)

Figure 4: Structure of 2H MS_2 monolayers (a) $BT_H(8,3,4)$ (b) $P_H(6,5)$

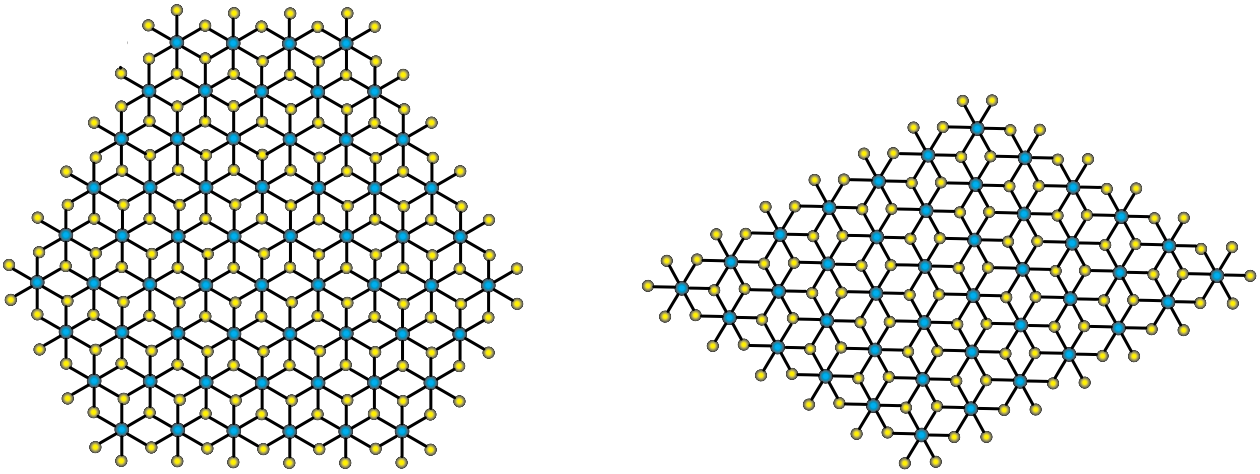

(a) (b)

Figure 5: Structure of 1T MS_2 monolayers (a) $BT_T(8,3,4)$ (b) $P_T(6,5)$

We now briefly explain the computational procedure to find the relativistic topological indices, in particular explaining the Θ-classes and their decomposition behaviors. The Θ-classes of these structures are grouped into four categories as horizontal $H_{\pm i}^{j\#}$, acute $A_{\pm i}^{j\#}$, obtuse $O_{\pm i}^{j\#}$ and pendant $P_i^{j\#}$ as depicted in Figure 6, where $\# \in \{b,h,p\}$ denotes the geometry of the structure and $i \in I$, the index set of Θ-classes. The quotient graph of all Θ-classes is a complete graph on two vertices with the vertex strength-weights $(X_{ki}^{j\#}(w), X_{ki}^{j\#}(s))$, $k = 1,2$ and edge strength-weights as $(X_{3i}^{j\#}(w^+)/X_{3i}^{j\#}(w^*), X_{3i}^{j\#}(s))$, $X \in \{H,A,O,P\}$ as in Figure 7. The relativistic topological characterization of the structures $BT_j(n,p,q)$, and $P_j(p,q)$ along with the detailed proof is given in the appendix section. Since the hexagonal shape is a particular case of bitrapezium, the relativistic topological indices of the structure $H_j(k)$ can be easily deduced from that of bitrapezium shape and

is presented as follows. It should be noted that the geometry of the bitrapezium graph structure $BT_H(n,p,q)$ possess complications in MATLAB interface while calculating the Mostar indices. Thus we limit the evaluation of various Mostar indices to the hexagonal shape MS_2 monolayer.

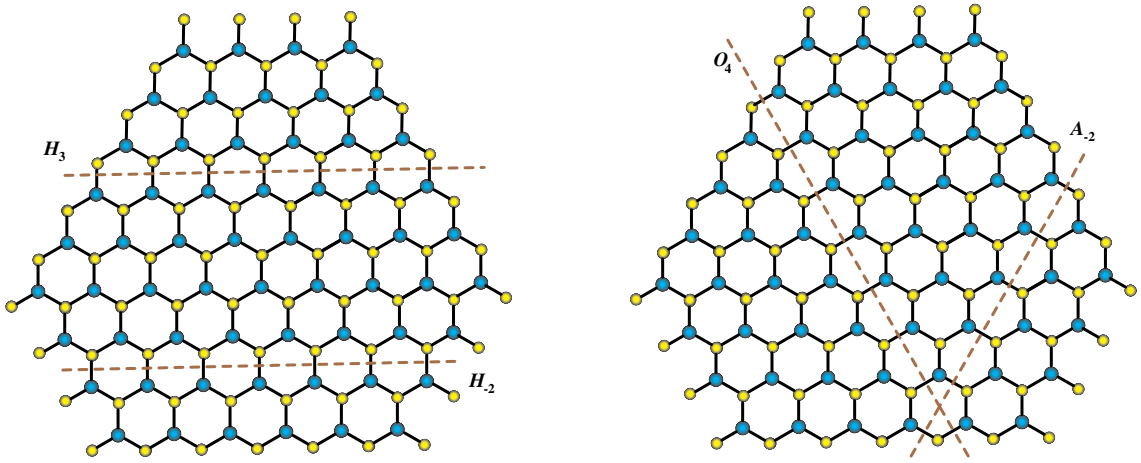

(a) (b)

Figure 6: Various Θ-classes of $BT_H(8,3,4)$

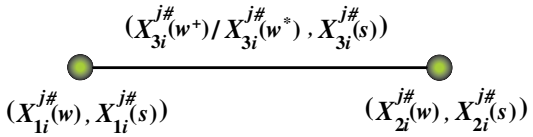

Figure 7: Quotient graph of Θ-class where $j \in \{H,T\}$

Theorem 4. *For hexagonal shape 2H MS_2 monolayer $H_H(k)$, we have*

1. $W(H_H(k)) = \frac{1}{10}k\{\gamma_M^2(82k^4-20k^2-2)+\gamma_M\gamma_S(164k^4+205k^3-4-25k+20k^2)+\gamma_S^2(82k^4+205k^3+140k^2+35k-42)\}$.

2. $W_e(H_H(k)) = \frac{3}{10}k(2k-1)\rho_{MS}^2\{123k^3-6k^2+2k+1\}$.

3. $W_{ve}(H_H(k)) = \frac{1}{20}k\rho_{MS}\{\gamma_M(492k^4-50k^2-135k^3-7)+\gamma_S(480k^3+492k^4-37-15k-50k^2)\}$.

4. $Sz_v(H_H(k)) = \frac{1}{20}k\rho_{MS}\{\gamma_M^2(270k^5-25k^3-5k)+\gamma_M\gamma_S(540k^5+4+160k^2-90k^3+646k^4)+\gamma_S^2(270k^5+646k^4+245k^3+100k^2+175k-56)\}$.

5. $Sz_e(H_H(k)) = \frac{3}{2}k^2\rho_{MS}^3\{81k^4-42k^3+10k^2-3k+2\}$.

6. $Sz_{ev}(H_H(k)) = \frac{1}{40}k\rho_{MS}^2\{\gamma_M(5k-30k^2+25k^3-420k^4+1620k^5)+\gamma_S(570k^2-48-5k-655k^3+1518k^4+1620k^5)\}$.

7. $PI(H_H(k)) = k\rho_{MS}^2\{81k^3 - 14k^2 + 3k - 4\}$.

8. $S(H_H(k)) = \frac{1}{5}k\rho_{MS}\{\gamma_M(492k^4 - 50k^2 - 7) + \gamma_S(85k^2 - 37 - 15k + 615k^3 + 492k^4)\}$.

9. $Gut(H_H(k)) = \frac{1}{5}k\rho_{MS}^2\{1476k^4 - 10k^2 + 15k - 26\}$.

10. $Mo(H_H(k)) = \frac{1}{2}k\rho_{MS}\{\gamma_M(27k^3 + 3k) + \gamma_S(27k^3 + 16k^2 - 3k - 16)\}$.

11. $Mo_e(H_H(k)) = \frac{3}{2}k\rho_{MS}^2\{27k^3 - 5k - 2\}$.

12. $Mo_t(H_H(k)) = \frac{1}{2}k\rho_{MS}\{\rho_{MS}(81k^3 - 15k - 6) + \gamma_M(27k^3 + 3k) + \gamma_S(27k^3 + 16k^2 - 3k - 16)\}$.

13. $w^+Mo(H_H(k)) = \frac{1}{5}k\rho_{MS}^2\{\gamma_M(564k^4 - 405k^3 + 330k^2 - 15k + 6) + \gamma_S(564k^4 - 75k^3 - 290k^2 + 135k - 94)\}$.

14. $w^+Mo_e(H_H(k)) = \frac{3}{5}k\rho_{MS}^3\{564k^4 - 405k^3 + 90k^2 + 25k - 14\}$.

15. $w^+Mo_t(H_H(k)) = \frac{1}{5}k\rho_{MS}^2\{\rho_{MS}(1692k^4 - 1215k^3 + 270k^2 + 75k - 42) + \gamma_M(564k^4 - 405k^3 + 330k^2 - 15k + 6) + \gamma_S(564k^4 - 75k^3 - 290k^2 + 135k - 94)\}$.

16. $w^*Mo(H_H(k)) = \frac{3}{5}k\rho_{MS}^3\{\gamma_M(282k^4 - 270k^3 + 165k^2 - 15k + 3) + \gamma_S(282k^4 - 105k^3 - 185k^2 + 75k - 7)\}$.

17. $w^*Mo_e(H_H(k)) = \frac{9}{5}k\rho_{MS}^4\{282k^4 - 270k^3 + 45k^2 + 25k - 2\}$.

18. $w^*Mo_t(H_H(k)) = \frac{3}{5}k\rho_{MS}^3\{\rho_{MS}(846k^4 - 810k^3 + 135k^2 + 75k - 6) + \gamma_M(282k^4 - 270k^3 + 165k^2 - 15k + 3) + \gamma_S(282k^4 - 105k^3 - 185k^2 + 75k - 7)\}$

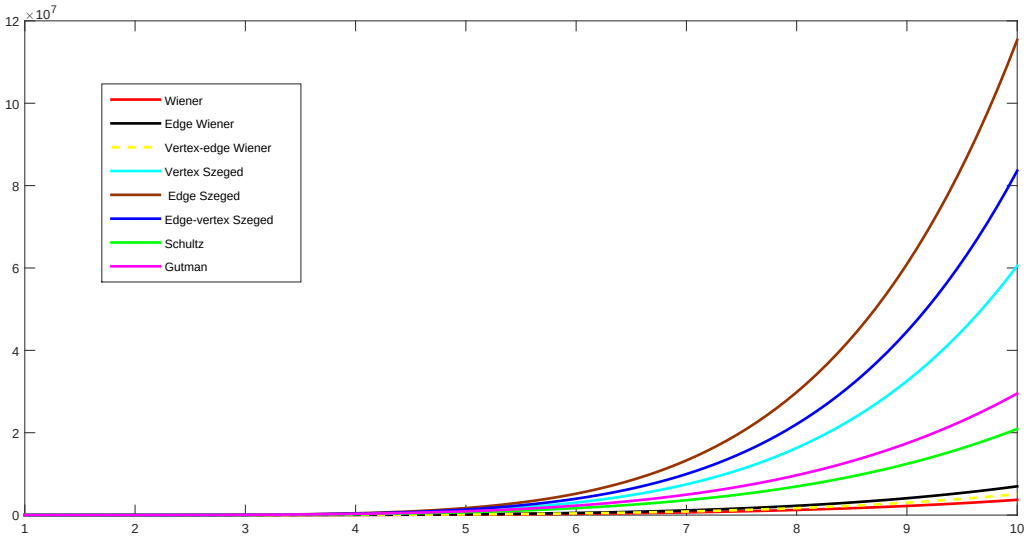

Figure 8: Comparative analysis of distance-based and Szeged-type indices for hexagonal shaped 2H MS_2 monolayers

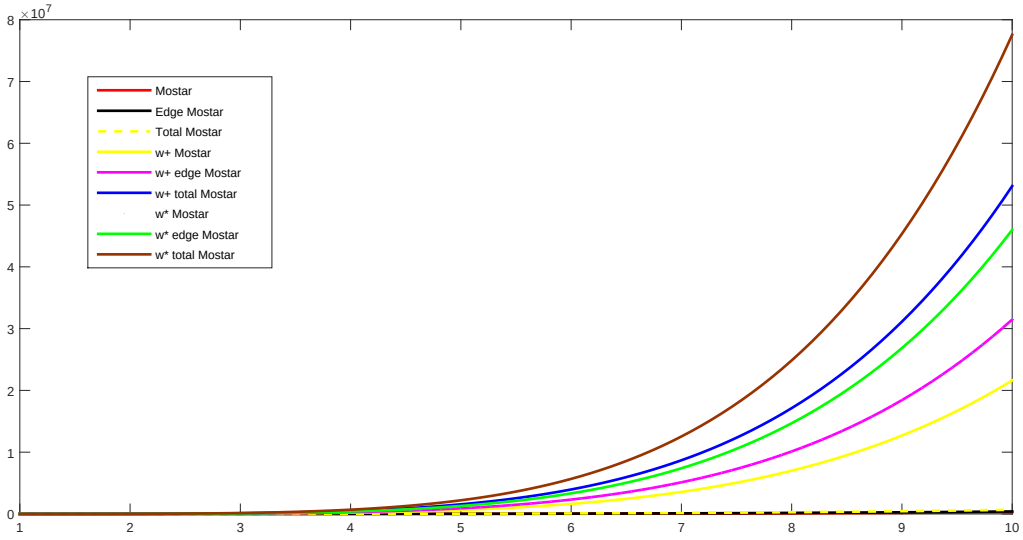

Figure 9: Comparative analysis of Mostar-type indices for hexagonal shaped 2H MS_2 monolayers

Theorem 5. *For hexagonal shape 1T MS_2 monolayer $H_T(k)$, we have*

1. $W(H_T(k)) = \frac{1}{5}k\{\gamma_M^2(41k^4 - 10k^2 - 1) + \gamma_M\gamma_S(164k^4 + 50k^2 - 10k + 205k^3 - 4) + \gamma_S^2(164k^4 + 410k^3 + 370k^2 + 175k + 21)\}$.

2. $W_e(H_T(k)) = \frac{1}{5}k\rho_{MS}^2\{1476k^4 - 810k^3 + 130k^2 - 15k - 31\}$.

3. $W_{ve}(H_T(k)) = \frac{1}{10}k\rho_{MS}\{\gamma_M(492k^4 - 7 - 50k^2 - 135k^3) + \gamma_S(15k - 14 + 170k^2 + 960k^3 + 984k^4)\}$.

4. $Sz_v(H_T(k)) = \frac{1}{10}k\rho_{MS}\{\gamma_M^2(270k^5 - 75k^3 - 15k) + \gamma_M\gamma_S(1080k^5 - 200k^2 - 60k - 210k^3 - 12 + 1292k^4) + \gamma_S^2(1080k^5 + 2584k^4 + 1300k^3 - 160k^2 - 130k + 6)\}$.

5. $Sz_e(H_T(k)) = 3k\rho_{MS}^3\{324k^5 - 168k^4 - 12k^3 + 22k^2 - 15k - 1\}$.

6. $Sz_{ev}(H_T(k)) = \frac{3}{20}k\rho_{MS}^2\{\gamma_M(40k^2 - 195k^3 - 280k^4 + 1080k^5 - 45k) + \gamma_S(6 + 30k - 240k^2 - 770k^3 + 2024k^4 + 2160k^5)\}$.

7. $PI(H_T(k)) = 4k\rho_{MS}^2\{81k^3 - 14k^2 + 3k + 2\}$.

8. $S(H_T(k)) = \frac{2}{5}k\rho_{MS}\{\gamma_M(492k^4 - 7 - 50k^2) + \gamma_S(60k - 14 + 440k^2 + 1230k^3 + 984k^4)\}$.

9. $Gut(H_T(k)) = \frac{12}{5}k\rho_{MS}^2\{492k^4 + 20k^2 - 7\}$.

10. $Mo(H_T(k)) = k\rho_{MS}\{\gamma_M(27k^3 + 9k) + \gamma_S(54k^3 + 32k^2 + 30k + 10)\}$.

11. $Mo_e(H_T(k)) = 18k^2\rho_{MS}^2(9k^2 + 2)$.

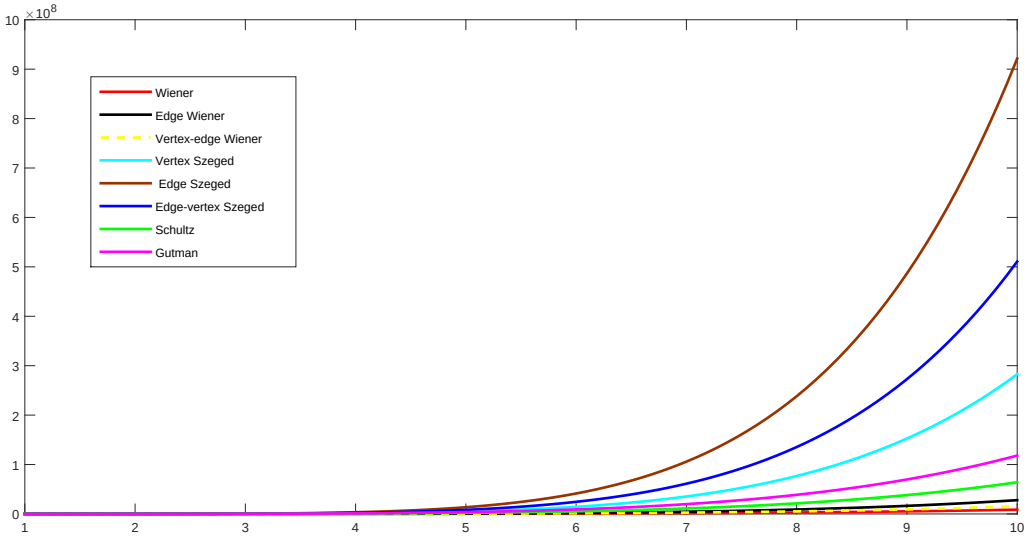

Figure 10: Comparative analysis of distance-based and Szeged-type indices for hexagonal shaped 1T MS_2 monolayers

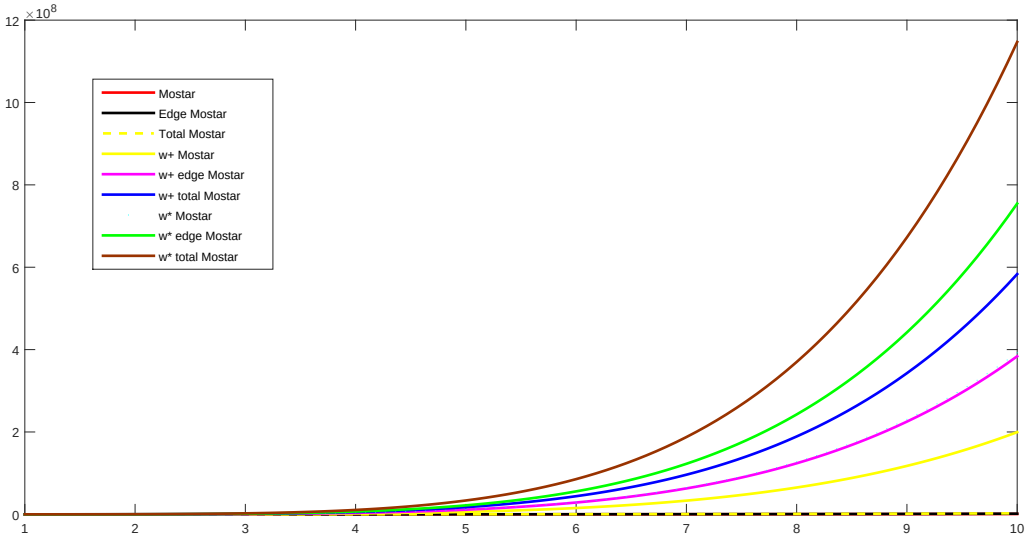

Figure 11: Comparative analysis of Mostar-type indices for hexagonal shaped 1T MS_2 monolayers

12. $Mo_t(H_T(k)) = k\rho_{MS}\{\rho_{MS}(162k^3 + 36k) + \gamma_M(27k^3 + 9k) + \gamma_S(54k^3 + 32k^2 + 30k + 10)\}$.

13. $w^+Mo(H_T(k)) = \frac{2}{5}k\rho_{MS}^2\{\gamma_M(1692k^4 - 945k^3 + 360k^2 - 45k - 27) + \gamma_S(3384k^4 + 90k^3 - 520k^2 + 300k + 166)\}$.

14. $w^+Mo_e(H_T(k)) = \frac{36}{5}k\rho_{MS}^3\{564k^4 - 315k^3 + 50k^2 + 5k + 1\}$.

15. $w^{+}Mo_t(H_T(k)) = \frac{2}{5}k\rho_{MS}^2\{\rho_{MS}(10152k^4 - 5670k^3 + 900k^2 + 90k + 18) + \gamma_M(1692k^4 - 945k^3 + 360k^2 - 45k - 27) + \gamma_S(3384k^4 + 90k^3 - 520k^2 + 300k + 166)\}$.

16. $w^{*}Mo(H_T(k)) = \frac{12}{5}k\rho_{MS}^3\{\gamma_M(564k^4 - 405k^3 + 120k^2 - 45k - 9) + \gamma_S(1128k^4 - 150k^3 - 280k^2 + 22)\}$.

17. $w^{*}Mo_e(H_T(k)) = \frac{72}{5}k\rho_{MS}^4\{564k^4 - 405k^3 + 50k^2 - 15k + 1\}$.

18. $w^{*}Mo_t(H_T(k)) = \frac{12}{5}k\rho_{MS}^3\{\rho_{MS}(3384k^4 - 2430k^3 + 300k^2 - 90k + 6) + \gamma_M(564k^4 - 405k^3 + 120k^2 - 45k - 9) + \gamma_S(1128k^4 - 150k^3 - 280k^2 + 22)\}$.

A comparative analysis of various topological indices of hexagonal shaped MS_2 monolayers in 2H phase is depicted in Figures 8 and 9 and that of MS_2 monolayers in 1T phase is depicted in Figures 10 and 11.

4 Applications of Computed Topological Indices

The various analytical expressions for the topological indices computed here can be valuable in structure-property predictions of the materials considered here, especially when combined with electronic parameters derived from quantum computations. Quantum computations typically yield the low-lying electronic energy levels, electron densities, equilibrium geometries, vibrational spectra and various electronic based indices or properties such as molecular electrostatic potentials, NBO parameters, Laplacians of charge densities, etc. From these parameters one could obtain quantitative measures of the relative stabilities, reactivities, and optical properties. Some of the electronic parameters that can be derived from quantum computations are shown below:

$$\begin{aligned} \chi &= (I + A)/2, \\ \eta &= (I - A)/2, \\ S &= 1/(2\eta), \\ \omega &= \mu^2/(2\eta), \end{aligned}$$

where I and A are ionization potential and electron affinity, χ is the electronegativity, η is the molecular hardness, S is the softness, ω is the electrophilicity index and μ is the chemical potential which is simply the negative of χ. In addition parameters such as polarizability can be computed quantum chemically.

The topological indices such as the Szeged index can also be used without extensive quantum computations for correlation with material properties such as dermal penetration, protonation constants,

chromatographic retention indices, lipophilicity, octanol partition coefficients, and so on. For example, the lipophiliticity index correlates with the Sz for polyacenes L_h as per the following expression [44]:

$$logP(L_h) = 1.0875 \times 10^{-4} Sz + 9.210,$$

where Sz is the Szeged index, and the statistical correlation with the observed property as measured by $R = 0.93$. Although the above expression is for certain polyacene molecular systems, similar expressions can be derived for materials under consideration, when there exists sufficient data set of observed properties.

In previous studies [45–47] for molecular systems containing very heavy atoms such as Pt_2 +H, Pd_3 and LaC_2, it has been shown how thermodynamic, vibrational, optical, and electronic properties can be obtained through relativistic quantum computations. Moreover vibrational modes of large systems such as the ones considered here can be computed through efficient use of topologically based partitioning of the vertices through group theoretical analysis and distance degree based vector sequences as demonstrated for $C_{48}N_{12}$ vibrational modes [48]. Distance and degree based topological sequences offer efficient alternatives for the vibrational spectroscopic analysis through vertex partitioning and thus offering significant simplifications in vibrational mode analysis. Mostar indices computed here provide insights into peripheral shapes of the materials in different phases. That is, the larger the Mostar index of a phase, the greater is the peripheral imperfection with zero Mostar index, resulting in peripheral perfection. Many properties such as dermal penetrations of nanomaterials and 2D sheets often depend on peripheral measures, molar volumes, etc., combined with other measures such as octanol partition coefficients. Consequently, the topological indices developed here can serve as useful tools in augmenting quantum computations and other electronic and reactivity based indices derivable from quantum computations.

5 Concluding Remarks

We have obtained the relativistic topological indices of two novel 2D transition metal disulfide monolayer materials in their two significant structural phases. We have shown that their graphs belong to a family of partial cubes, a class of graphs whose metric structure is well-understood. The Mostar type indices are hard to produce in closed forms for generalized bitrapezium shapes of MS_2 monolayers due to some setbacks in finding the absolute differences using the MATLAB interface, whereas a script file can be easily generated from our computations to find the Mostar indices of a particular structure. As the present model includes relativistic quantum effects, it is anticipated that the newly developed model will provide greater insights into the molecular structures and 2D networks of these

novel materials. This better understanding of the geometries and behaviors of these high performance thermoelectric materials will enable us to expand their applications in the emerging technology, since the study on their opto-electronic properties is a new, exciting and rapidly growing area of research.

Acknowledgement

S. Klavžar acknowledges the financial support from the Slovenian Research Agency (research core funding No. P1-0297 and projects J1-9109, J1-1693, N1-0095, N1-0108).

References

[1] M. Xu, T. Liang, M. Shi, H. Chen, Graphene-like two-dimensional materials, Chem. Rev. **113** (2013) 3766–3798.

[2] H. Babaei, J.M. Khodadadi, S. Sinha, Large theoretical thermoelectric power factor of suspended single-layer MoS_2, Appl. Phys. Lett. **105** (2014) 193901.

[3] V. Carozo, Y. Wang, K. Fujisawa, B.R. Carvalho, A. McCreary, S. Feng, Z. Lin, C. Zhou, N. Perea-López, A.L. Elías, B. Kabius, V.H. Crespi, M. Terrones, Optical identification of sulfur vacancies: Bound excitons at the edges of monolayer tungsten disulfide, Sci. Adv. **3**(4) (2017) e1602813.

[4] A. Kuc, N. Zibouche, T. Heine, Influence of quantum confinement on the electronic structure of the transition metal sulfide TS_2, Phys. Rev. B **83** (2011) 245213.

[5] K.F. Mak, J. Shan, Photonics and optoelectronics of 2D semiconductor transition metal dichalcogenides, Nat. Photonics **10** (2016) 216–226.

[6] Y. Zhang, Y. Zhang, Q. Ji, J. Ju, H. Yuan, J. Shi, T. Gao, D. Ma, M. Liu, Y. Chen, X. Song, H.Y. Hwang, Y. Cui, Z. Liu, Controlled growth of high-quality monolayer WS_2 layers on sapphire and imaging its grain boundary, ACS Nano **7**(10) (2013) 8963–8971.

[7] D. Xiao, G.-B. Liu, W. Feng, X. Xu, W. Yao, Coupled spin and valley physics in monolayers of MoS_2 and other group-VI dichalcogenides, Phys. Rev. Lett. **108** (2012) 196802.

[8] H. Jiang, Electronic band structures of molybdenum and tungsten dichalcogenides by the GW approach, J. Phys. Chem. C **116**(14) (2012) 7664–7671.

[9] K. Balasubramanian, Relativistic effects in chemistry, Part A: Theory and techniques, Wiley, New York, 1997.

[10] K. Balasubramanian, Spectroscopic constants and potential energy curves of tungsten carbide, J. Chem. Phys. **112**(17) (2000) 7425–7436.

[11] H. Hwang, H. Kim, J. Cho, MoS_2 nanoplates consisting of disordered graphene-like layers for high rate lithium battery anode materials, Nano Lett. **11** (2011) 4826–4830.

[12] S. Bertolazzi, J. Brivio, A. Kis, Stretching and breaking of ultrathin MoS_2, ACS Nano **5** (2011) 9703–9709.

[13] G. Eda, H. Yamaguchi, D. Voiry, T. Fujita, M. Chen, M. Chhowalla, Photoluminescence from chemically exfoliated MoS_2, Nano Lett. **11**(12) (2011) 5111–5116.

[14] K. Mak, K. He, J. Shan, T.F. Heinz, Control of valley polarization in monolayer MoS_2 by optical helicity, Nat. Nanotechnol. **7** (2012) 494–498.

[15] S. Manzeli, D. Ovchinnikov, D. Pasquier, O.V. Yazyev, A. Kis, 2D transition metal dichalcogenides, Nat. Rev. Mater. **2** (2017) 17033.

[16] G.S.B. McKee, K.S. Vecchio, Thermogravimetric analysis of synthesis variation effects on CVD generated multiwalled carbon nanotubes, J. Phys. Chem. B **110**(3) (2006) 1179–1186.

[17] K. Momeni, Y. Ji, Y. Wang, S. Paul, S. Neshani, D.E. Yilmaz, Y.K. Shin, D. Zhang, J.W. Jiang, H.S. Park, S. Sinnott, A.v. Duin, V. Crespi, L.-Q. Chen, Multiscale computational understanding and growth of 2D materials: A review, npj Comput. Mater. **6** (2020) 22.

[18] S. Paul, K. Momeni, V.I. Levitas, Shear-induced diamondization of multilayer graphene structures: A computational study, Carbon **167** (2020) 140–147.

[19] M. Arockiaraj, J. Clement, N. Tratnik, S. Mushtaq, K. Balasubramanian, Weighted Mostar indices as measures of molecular peripheral shapes with applications to graphene, graphyne and graphdiyne nanoribbons, SAR QSAR Environ. Res. **31**(3) (2020) 187–208.

[20] K.Q. Dang, D.E. Spearot, Effect of point and grain boundary defects on the mechanical behavior of monolayer MoS_2 under tension via atomistic simulations, J. Appl. Phys. **116**(1) (2014) 013508.

[21] K. Balasubramanian, Mathematical and computational techniques for drug discovery: Promises and developments, Curr. Top. Med. Chem. **18**(32) (2018) 2774–2799.

[22] R. Carbó-Dorca, T. Chakraborty, Divagations about the periodic table: Boolean hypercube and quantum similarity connections, J. Comput. Chem. **40**(30) (2019) 2653–2663.

[23] M. Arockiaraj, J. Clement, N. Tratnik, Mostar indices of carbon nanostructures and circumscribed donut benzenoid systems, Int. J. Quantum Chem. **119**(24) (2019) e26043.

[24] M. Arockiaraj, S. Klavžar, J. Clement, S. Mushtaq, K. Balasubramanian, Edge distance-based topological indices of strength-weighted graphs and their application to coronoid systems, carbon nanocones and SiO_2 nanostructures, Mol. Inform. **38**(11-12) (2019) 1900039.

[25] M. Arockiaraj, J. Clement, K. Balasubramanian, Topological indices and their applications to circumcised donut benzenoid systems, kekulenes and drugs, Polycycl. Aromat. Comp. **40**(2) (2018) 280–303.

[26] M. Črepnjak, N. Tratnik, The Szeged index and the Wiener index of partial cubes with applications to chemical graphs, Appl. Math. Comput. **309** (2017) 324–333.

[27] N. Tratnik, The edge-Szeged index and the PI index of benzenoid systems in linear time, MATCH Commun. Math. Comput. Chem. **77**(2) (2017) 393–406.

[28] T. Došlić, I. Martinjak, R. Škrekovski, S.T. Spužević, I. Zubac, Mostar index, J. Math. Chem. **56** (2018) 2995–3013.

[29] J.C. Dobrowolski, The structural formula version of graph theory, MATCH Commun. Math. Comput. Chem. **81** (2019) 527–555.

[30] M. Arockiaraj, S.R.J. Kavitha, S. Mushtaq, K. Balasubramanian, Relativistic topological molecular descriptors of metal trihalides, J. Mol. Struc. **1217** (2020) 128368.

[31] S. Klavžar, M.J. Nadjafi-Arani, Cut method: Update on recent developments and equivalence of independent approaches, Curr. Org. Chem. **19**(4) (2015) 348–358.

[32] M. Chhowalla, H.S. Shin, G. Eda, L.-J. Li, K.P. Loh, H. Zhang, The chemistry of two-dimensional layered transition metal dichalcogenide nanosheets, Nat. Chem. **5** (2013) 263–275.

[33] C. Ataca, H. Şahin, S. Ciraci, Stable, single-layer MX_2 transition-metal oxides and dichalcogenides in a honeycomb-like structure, J. Phys. Chem. C **116**(16) (2012) 8983–8999.

[34] F. Wypych, R. Schöllhorn, 1T-MoS_2, a new metallic modification of molybdenum-disulfide, J. Chem. Soc., Chem. Commun. **19** (1992) 1386–1388.

[35] P. Pyykko, Relativistic effects in structural chemistry, Chem. Rev. **88**(3) (1988) 563–594.

[36] K. Balasubramanian, Relativistic calculations of electronic states and potential energy surfaces of Sn_3, J. Chem. Phys. **85**(6) (1986) 3401–3406.

[37] K. Balasubramanian, Group theoretical treatment of Jahn-Teller versus spin-orbit effects on geometries, rovibronic levels and nuclear spin species of bismuth and antimony clusters, Mol. Phys. **107**(8-12) (2009) 797–807.

[38] J. Pipek, P.G. Mezey, A fast intrinsic localization procedure applicable for ab initio and semiempirical linear combination of atomic orbital wave functions, J. Chem. Phys. **90**(9) (1989) 4916–4926.

[39] Q. Tang, D.E. Jiang, Stabilization and band-gap tuning of the 1T-MoS_2 monolayer by covalent functionalization, Chem. Mater. **27** (2015) 3743–3748.

[40] H. Huang, Y. Cui, Q. Li, C. Dun, W. Zhou, W. Huang, L. Chen, C.A. Hewitt, D.L. Carroll, Metallic 1T phase MoS_2 nanosheets for high-performance thermoelectric energy harvesting, Nano Energy **26** (2016) 172–179.

[41] V. Chepoi, d-Convexity and isometric subgraphs of Hamming graphs, Cybernetics **24**(1) (1988) 6–11.

[42] W. Zhou, X. Zou, S. Najmaei, Z. Liu, Y. Shi, J. Kong, J. Lou, P.M. Ajayan, B.I. Yakobson, J.-C. Idrobo, Intrinsic structural defects in monolayer molybdenum disulfide, Nano Lett. **13**(6) (2013) 2615–2622.

[43] M.A. Lukowski, A.S. Daniel, F. Meng, A. Forticaux, L. Li, S. Jin, Enhanced hydrogen evolution catalysis from chemically exfoliated metallic MoS_2 nanosheets, J. Am. Chem. Soc. **135**(28) (2013) 10274–10277.

[44] P.V. Khadikar, S. Karmarkar, V.K. Agrawal, J. Singh, A. Shrivastava, I. Lukovits, M.V. Diudea, Szeged index-applications for drug modelling, Lett. Drug Des. Discov. **2**(8) (2005) 606–624.

[45] K. Balasubramanian, P.Y. Feng, Potential-energy surfaces for Pt_2+H and Pt+H interactions, J. Chem. Phys. (1990) 541–550.

[46] K. Balasubramanian, Ten low-lying electronic states of Pd_3, J. Chem. Phys. **91**(1) (1989) 307–313.

[47] S. Roszak, K. Balasubramanian, Theoretical investigation of structural and thermodynamic properties of lanthanum carbides LaC_n (n= 2-6), J. Chem. Phys. **106**(1) (1997) 158–164.

[48] K. Balasubramanian, Group theoretical analysis of vibrational modes and rovibronic levels of extended aromatic $C_{48}N_{12}$ azafullerene, Chem. Phys. Lett. **391**(1-3) (2004) 64–68.

Appendix

The analytical expressions of various relativistic topological indices for the structures $BT_H(n,p,q)$, $BT_T(n,p,q)$, $P_H(p,q)$, $P_T(p,q)$ are derived in a detailed manner in the following.

Theorem 6. *For bitrapezium shape 2H MS_2 monolayer $BT_H(n,p,q)$, $p+q \leq n$, we have*

1. $W(BT_H(n,p,q)) = \frac{1}{60}\{\gamma_S^2(20n^3p^2+40n^3pq+120n^3p+20n^3q^2+120n^3q+180n^3-20n^2p^3+90n^2p^2+240n^2pq+710n^2p-20n^2q^3-30n^2q^2+350n^2q+840n^2+10np^4-60np^3+120np^2+440npq+1290np+10nq^4+20nq^3+370nq+1140n-4p^5-10p^4q-15p^4-20p^3q-90p^3+10p^2q+195p^2-10pq^4-100pq^3-350pq^2-240pq+634p-4q^5-35q^4-170q^3-385q^2-246q+360)+\gamma_M^2(20n^3p^2+40n^3pq+80n^3p+20n^3q^2+80n^3q+80n^3-20n^2p^3+30n^2p^2+120n^2pq+230n^2p-20n^2q^3-30n^2q^2+110n^2q+180n^2+10np^4-20np^3+80npq+150np+10nq^4+20nq^3+50nq+100n-4p^5-10p^4q-15p^4-20p^3q-30p^3+10p^2q+15p^2-10pq^4-60pq^3-110pq^2-40pq+34p-4q^5-25q^4-70q^3-95q^2-46q)+\gamma_M\gamma_S(40n^3p^2+80n^3pq+200n^3p+40n^3q^2+200n^3q+240n^3-40n^2p^3+120n^2p^2+360n^2pq+880n^2p-40n^2q^3-60n^2q^2+460n^2q+840n^2+20np^4-80np^3+90np^2+460npq+1110np+20nq^4+40nq^3-30nq^2+390nq+900n-8p^5-20p^4q-30p^4-40p^3q-130p^3+20p^2q+30p^2-20pq^4-160pq^3-430pq^2-250pq+318p-8q^5-60q^4-220q^3-450q^2-282q+180)\}$.

2. $W_e(BT_H(n,p,q)) = \frac{3}{40}\rho_{MS}^2\{40n^3p^2+80n^3pq+160n^3p+40n^3q^2+160n^3q+160n^3-40n^2p^3+120n^2pq+240n^2p-40n^2q^3-120n^2q^2+160n^2+20np^4+20np^3+60np^2q+80np^2+60npq^2+240npq+240np+20nq^4+100nq^3+200nq^2+240nq+160n-8p^5-20p^4q-45p^4-40p^3q-50p^3-30p^2q^2-50p^2q+5p^2-20pq^4-120pq^3-230pq^2-130pq+18p-8q^5-65q^4-190q^3-235q^2-102q\}$.

3. $W_{ev}(BT_H(n,p,q)) = \frac{1}{80}\rho_{MS}\{\gamma_M(360n+86p-194q+520n^2+320n^3+35p^2-110p^3-75p^4-16p^5-425q^2-330q^3-115q^4-16q^5+80np^2+700n^2p-20np^3+320n^3p+40np^4+200nq^2+220n^2q+140nq^3+320n^3q+40nq^4-450pq^2-30p^2q-240pq^3-80p^3q-40pq^4-40p^4q+60n^2p^2-80n^2p^3+80n^3p^2-180n^2q^2-80n^2q^3+80n^3q^2-30p^2q^2+540np+340nq-210pq+400npq+60npq^2+60np^2q+360n^2pq+160n^3pq)+\gamma_S(240+1400n+526p-474q+1360n^2+480n^3+135p^2-210p^3-75p^4-16p^5-845q^2-490q^3-135q^4-16q^5+220np^2+1460n^2p-100np^3+400n^3p+40np^4+180nq^2+620n^2q+140nq^3+400n^3q+40nq^4-830pq^2-30p^2q-320pq^3-80p^3q-40pq^4-40p^4q+180n^2p^2-80n^2p^3+80n^3p^2-180n^2q^2-80n^2q^3+80n^3q^2-30p^2q^2+1840np+760nq-510pq+920npq+60npq^2+60np^2q+600n^2pq+160n^3pq)\}$.

4. $Sz_v(BT_H(n,p,q)) = \frac{1}{240}\rho_{MS}\{\gamma_M^2(120n^3p^3+360n^3p^2q+720n^3p^2+360n^3pq^2+1440n^3pq+1400n^3p+120n^3q^3+720n^3q^2+1400n^3q+880n^3-180n^2p^4-360n^2p^3q-560n^2p^3-360n^2p^2q^2-600n^2p^2q+300n^2p^2-360n^2pq^3-840n^2pq^2+840n^2pq+2120n^2p-180n^2q^4-880n^2q^3-900n^2q^2+1000n^2q+1440n^2+90np^5+90np^4q-20np^4+180np^3q^2-120np^3q-1010np^3+180np^2q^3+360np^2q^2-$

$630np^2q-1180np^2+90npq^4+120npq^3-390npq^2-360npq+360np+90nq^5+380nq^4+190nq^3-620nq^2-120nq+560n-15p^6+73p^5-45p^4q^2+75p^4q+345p^4+110p^3q^2+430p^3q+335p^3-45p^2q^4-110p^2q^3+270p^2q^2+695p^2q+150p^2-75pq^4-370pq^3-455pq^2+72p-15q^6-73q^5-135q^4-255q^3-450q^2-272q)+\gamma_S^2(120n^3p^3+360n^3p^2q+1000n^3p^2+360n^3pq^2+2000n^3pq+2480n^3p+120n^3q^3+1000n^3q^2+2480n^3q+1920n^3-180n^2p^4-360n^2p^3q-480n^2p^3-360n^2p^2q^2-240n^2p^2q+2340n^2p^2-360n^2pq^3-840n^2pq^2+4080n^2pq+8400n^2p-180n^2q^4-1160n^2q^3-660n^2q^2+5120n^2q+6720n^2+90np^5+90np^4q-330np^4+180np^3q^2-480np^3q-2670np^3+180np^2q^3+180np^2q^2-1650np^2q-1870np^2+90npq^4-240npq^3-2490npq^2+460npq+6700np+90nq^5+430nq^4-790nq^3-3470nq^2+1100nq+6480n-15p^6+179p^5-45p^4q^2+115p^4q+565p^4+290p^3q^2+610p^3q-515p^3-45p^2q^4-110p^2q^3+570p^2q^2+715p^2q-910p^2+55pq^4-150pq^3-1785pq^2-1660pq+1416p-15q^6-57q^5+185q^4-15q^3-2210q^2-1968q+1440)+\gamma_M\gamma_S(240n^3p^3+720n^3p^2q+1720n^3p^2+720n^3pq^2+3440n^3pq+3800n^3p+240n^3q^3+1720n^3q^2+3800n^3q+2640n^3-360n^2p^4-720n^2p^3q-1040n^2p^3-720n^2p^2q^2-840n^2p^2q+2280n^2p^2-720n^2pq^3-1680n^2pq^2+4440n^2pq+9200n^2p-360n^2q^4-2040n^2q^3-1680n^2q^2+5280n^2q+6720n^2+180np^5+180np^4q-350np^4+360np^3q^2-600np^3q-3600np^3+360np^2q^3+540np^2q^2-2280np^2q-3290np^2+180npq^4-120npq^3-2400npq^2-140npq+4900np+180nq^5+810nq^4-360nq^3-3370nq^2+820nq+5040n-30p^6+252p^5-90p^4q^2+190p^4q+970p^4+400p^3q^2+1040p^3q+140p^3-90p^2q^4-220p^2q^3+840p^2q^2+1410p^2q-820p^2-20pq^4-680pq^3-2120pq^2-1380pq+448p-30q^6-130q^5-50q^4-470q^3-2440q^2-1920q+720)\}$.

5. $Sz_e(BT_H(n,p,q))=\frac{1}{80}\rho_{MS}^3\{360n^3p^3+1080n^3p^2q+2040n^3p^2+1080n^3pq^2+4080n^3pq+3840n^3p+360n^3q^3+2040n^3q^2+3840n^3q+2400n^3-540n^2p^4-1080n^2p^3q-1720n^2p^3-1080n^2p^2q^2-2280n^2p^2q-420n^2p^2-1080n^2pq^3-3120n^2pq^2-480n^2pq+2920n^2p-540n^2q^4-2720n^2q^3-3900n^2q^2-280n^2q+1920n^2+270np^5+270np^4q+140np^4+540np^3q^2+360np^3q-1270np^3+540np^2q^3+1680np^2q^2+750np^2q-980np^2+270npq^4+840npq^3+1110npq^2+1800npq+1600np+270nq^5+1300nq^4+1970nq^3+1340nq^2+1600nq+1440n-45p^6+131p^5-135p^4q^2-15p^4q+445p^4+130p^3q^2+450p^3q+345p^3-135p^2q^4-490p^2q^3-330p^2q^2+145p^2q-160p^2-225pq^4-1270pq^3-2185pq^2-1220pq-236p-45q^6-251q^5-695q^4-1465q^3-1900q^2-924q\}$.

6. $Sz_{ev}(BT_H(n,p,q))=\frac{1}{240}\rho_{MS}^2\{\gamma_M(1560n-10p-870q+3120n^2+2520n^3+145p^2+675p^3+740p^4+175p^5-45p^6-1625q^2-1115q^3-550q^4-235q^5-45q^6-2260np^2+4640n^2p-2150np^3+4020n^3p+40np^4+270np^5-260nq^2+1360n^2q+1270nq^3+4020n^3q+1220nq^4+270nq^5-1775pq^2+1115p^2q-1190pq^3+870p^3q-225pq^4+105p^4q+240n^2p^2-1700n^2p^3+2100n^3p^2-540n^2p^4+360n^3p^3-3300n^2q^2-2680n^2q^3+2100n^3q^2-540n^2q^4+360n^3q^3+240p^2q^2-410p^2q^3+230p^3q^2-135p^2q^4-135p^4q^2+1340np+620nq-610pq+360npq-1080n^2p^2q^2-30npq^2-570np^2q+1020n^2pq+600npq^3+4200n^3pq+270npq^4+270np^4q+1380np^2q^2-2820n^2pq^2-2040n^2p^2q+540np^2q^3+$

$540np^3q^2 - 1080n^2pq^3 - 1080n^2p^3q + 1080n^3pq^2 + 1080n^3p^2q) + \gamma_S(720 + 5520n + 766p - 2094q + 8040n^2 + 3720n^3 - 345p^2 + 460p^3 + 1230p^4 + 334p^5 - 45p^6 - 2765q^2 - 635q^3 - 130q^4 - 211q^5 - 45q^6 - 4195np^2 + 11300n^2p - 4560np^3 + 5400n^3p - 425np^4 + 270np^5 - 3635nq^2 + 5620n^2q + 40nq^3 + 5400n^3q + 1295nq^4 + 270nq^5 - 2510pq^2 + 1865p^2q - 860pq^3 + 1300p^3q - 30pq^4 + 165p^4q + 2700n^2p^2 - 1580n^2p^3 + 2520n^3p^2 - 540n^2p^4 + 360n^3p^3 - 3060n^2q^2 - 3100n^2q^3 + 2520n^3q^2 - 540n^2q^4 + 360n^3q^3 + 930p^2q^2 - 410p^2q^3 + 500p^3q^2 - 135p^2q^4 - 135p^4q^2 + 5430np + 710nq - 1520pq - 210npq - 1080n^2p^2q^2 - 2700npq^2 - 2340np^2q + 4920n^2pq + 60npq^3 - 540np^3q + 5040n^3pq + 270npq^4 + 270np^4q + 1110np^2q^2 - 2820n^2pq^2 - 1500n^2p^2q + 540np^2q^3 + 540np^3q^2 - 1080n^2pq^3 - 1080n^2p^3q + 1080n^3pq^2 + 1080n^3p^2q)\}$.

7. $PI(BT_H(n,p,q)) = \frac{1}{4}\rho_{MS}^2\{36n^2p^2 + 72n^2pq + 140n^2p + 36n^2q^2 + 140n^2q + 140n^2 - 36np^3 - 36np^2q - 40np^2 - 36npq^2 - 16npq + 108np - 36nq^3 - 112nq^2 - 36nq + 100n + 9p^4 - 14p^3 + 18p^2q^2 + 26p^2q - 5p^2 - 10pq^2 - 2pq + 42p + 9q^4 + 22q^3 - 5q^2 - 18q + 24\}$.

8. $S(BT_H(n,p,q)) = \frac{1}{10}\rho_{MS}\{\gamma_M(30 + 300n + 73p - 127q + 380n^2 + 160n^3 - 5p^2 - 70p^3 - 30p^4 - 8p^5 - 235q^2 - 150q^3 - 50q^4 - 8q^5 + 10np^2 + 470n^2p - 40np^3 + 160n^3p + 20np^4 + 10nq^2 + 230n^2q + 40nq^3 + 160n^3q + 20nq^4 - 240pq^2 - 120pq^3 - 40p^3q - 20pq^4 - 20p^4q + 60n^2p^2 - 40n^2p^3 + 40n^3p^2 - 60n^2q^2 - 40n^2q^3 + 40n^3q^2 + 390np + 170nq - 120pq + 200npq + 240n^2pq + 80n^3pq) + \gamma_S(210 + 970n + 353p - 297q + 860n^2 + 240n^3 + 30p^2 - 135p^3 - 30p^4 - 8p^5 - 475q^2 - 230q^3 - 60q^4 - 8q^5 + 95np^2 + 880n^2p - 80np^3 + 200n^3p + 20np^4 - 15nq^2 + 460n^2q + 40nq^3 + 200n^3q + 20nq^4 - 445pq^2 - 160pq^3 - 40p^3q - 20pq^4 - 20p^4q + 120n^2p^2 - 40n^2p^3 + 40n^3p^2 - 60n^2q^2 - 40n^2q^3 + 40n^3q^2 + 1175np + 425nq - 285pq + 490npq + 360n^2pq + 80n^3pq)\}$.

9. $Gut(BT_H(n,p,q)) = \frac{1}{10}\rho_{MS}{}^2\{120n^3p^2 + 240n^3pq + 480n^3p + 120n^3q^2 + 480n^3q + 480n^3 - 120n^2p^3 + 180n^2p^2 + 720n^2pq + 1430n^2p - 120n^2q^3 - 180n^2q^2 + 710n^2q + 1190n^2 + 60np^4 - 120np^3 + 50np^2 + 680npq + 1350np + 60nq^4 + 120nq^3 + 50nq^2 + 630nq + 1090n - 24p^5 - 60p^4q - 90p^4 - 120p^3q - 230p^3 - 40p^2q - 65p^2 - 60pq^4 - 360pq^3 - 760pq^2 - 440pq + 249p - 24q^5 - 150q^4 - 470q^3 - 785q^2 - 441q + 150)\}$.

Proof. The cardinality of structural vertex and edge sets of $BT_H(n,p,q))$ are given by $|V_\gamma(BT_H(n,p,q))| = (\gamma_M(2 + 4n + p - q - p^2 - q^2 + 2np + 2nq) + \gamma_S(6 + 6n + 3p - q - p^2 - q^2 + 2np + 2nq))/2$ and $|E_\rho(BT_H(n,p,q))| = 3\rho_{MS}(4n + p - q + 2np + 2nq - p^2 - q^2 + 2)/2$ while the total number of vertices and edges in the underlying graph are $5n + 2p - q + 2np + 2nq - p^2 - q^2 + 4$ and $3(4n + p - q + 2np + 2nq - p^2 - q^2 + 2)/2$ respectively.

As the Θ-classes $A_{\pm i}^{hb}$ and $O_{\pm i}^{hb}$ are symmetric to each other in $BT_H(n,p,q)$, it is sufficient to determine the strength-weighted parameters for the three types of Θ-classes. The computed values of the strength-weighted parameters of the quotient graphs are tabulated in Table 2 and in addition that $X_{2i}^{Hb}(w) = |V_\gamma(BT_H(n,p,q))| - X_{1i}^{Hb}(w)$ and $X_{2i}^{Hb}(s) = |E_\rho(BT_H(n,p,q))| - X_{1i}^{Hb}(s) - X_{3i}^{Hb}(s)$.

We thus evaluate the various indices $TI \in \{W, W_e, W_{ev}, Sz_v, Sz_e, Sz_{ev}, PI, S, Gut\}$ by substituting the above mentioned parameter values in the following expression,

$$\begin{aligned} TI(BT_H(n,p,q)) = &\sum_{i=1}^{q+1} TI(BT_H(n,p,q)/H_i^{Hb}) + \sum_{i=1}^{p} TI(BT_H(n,p,q)/H_{-i}^{Hb}) \\ &+ 2\sum_{i=1}^{p} TI(BT_H(n,p,q)/A_i^{Hb}) + 2\sum_{i=p+1}^{n-q} TI(BT_H(n,p,q)/A_i^{Hb}) \\ &+ 2\sum_{i=1}^{q} TI(BT_H(n,p,q)/A_{-i}^{Hb}) + \sum_{i=1}^{n-q+2(p+1)} TI(BT_H(n,p,q)/P_i^{Hb}). \end{aligned}$$

Table 2: Strength-weighted parameters of $BT_H(n,p,q)$

Θ-class	Edge-strength $X_{3i}^{Hb}(s)$	Vertex-weight $X_{1i}^{Hb}(w)$	Vertex-strength $X_{1i}^{Hb}(s)$
H_i^{Hb}:$1 \le i \le q+1$	$\rho_{MS}(n-q+i)$	$(\gamma_S(i+1)(i+2n-2q)+ i\gamma_M(i+2n-2q-1))/2$	$3i\rho_{MS}(i+2n-2q-1)/2$
H_{-i}^{Hb}:$1 \le i \le p$	$\rho_{MS}(n-p+i)$	$(i\gamma_M(i+2n-2p+1)+ i\gamma_S(i+2n-2p+3))/2$	$\rho_{MS}(i-2n+2p+6ni- 6ip+3i^2)/2$
A_i^{Hb}:$1 \le i \le p$	$\rho_{MS}(q+i+1)$	$(i\gamma_S(i+2q+5)+i\gamma_M(i+ 2q+3))/2$	$\rho_{MS}(7i-2q+6iq+3i^2- 2)/2$
A_i^{Hb}:$p+1 \le i \le n-q$	$\rho_{MS}(p+q+2)$	$(\gamma_S(6i-p-p^2+2ip+ 2iq)+\gamma_M(4i-p-p^2+ 2ip+2iq))/2$	$\rho_{MS}(12i-5p-2q+6ip+ 6iq-3p^2-4)/2$
A_{-i}^{Hb}:$1 \le i \le q$	$\rho_{MS}(p+i+1)$	$(\gamma_S(2(p+1)+i(i+2p+ 3))+i\gamma_M(i+2p+1))/2$	$3i\rho_{MS}(i+2p+1)/2$
P_i^{Hb}:$1 \le i \le n-q+2(p+1)$	ρ_{MS}	γ_S	0

□

Theorem 7. *For bitrapezium shape 1T MS_2 monolayer $BT_T(n,p,q)$, $p+q<n$, we have*

1. $W(BT_T(n,p,q)) = \frac{1}{60}\{\gamma_M^2(20n^3p^2+40n^3pq+80n^3p+20n^3q^2+80n^3q+80n^3-20n^2p^3+30n^2p^2+120n^2pq+230n^2p-20n^2q^3-30n^2q^2+110n^2q+180n^2+10np^4-20np^3+80npq+150np+10nq^4+20nq^3+50nq+100n-4p^5-10p^4q-15p^4-20p^3q-30p^3+10p^2q+15p^2-10pq^4-60pq^3-110pq^2-40pq+34p-4q^5-25q^4-70q^3-95q^2-46q)+\gamma_S^2(80n^3p^2+160n^3pq+480n^3p+80n^3q^2+480n^3q+720n^3-80n^2p^3+240n^2p^2+960n^2pq+2660n^2p-80n^2q^3+1940n^2q+3780n^2+40np^4-160np^3+$

$180np^2+1760npq+4480np+40nq^4-60nq^2+2760nq+6060n-16p^5-40p^4q-80p^4-160p^3q-440p^3-140p^2q-100p^2-40pq^4-320pq^3-860pq^2+120pq+2316p-16q^5-120q^4-600q^3-1200q^2+616q+3120)+\gamma_M\gamma_S(80n^3p^2+160n^3pq+400n^3p+80n^3q^2+400n^3q+480n^3-80n^2p^3+180n^2p^2+720n^2pq+1700n^2p-80n^2q^3-60n^2q^2+1100n^2q+1800n^2+40np^4-120np^3+60np^2+920npq+2060np+40nq^4+40nq^3-60nq^2+1060nq+2040n-16p^5-40p^4q-70p^4-120p^3q-270p^3-50p^2q-110p^2-40pq^4-280pq^3-650pq^2-200pq+646p-16q^5-110q^4-430q^3-850q^2-334q+540)\}$.

2. $W_e(BT_T(n,p,q))=\frac{1}{10}\rho_{MS}^2\{120n^3p^2+240n^3pq+480n^3p+120n^3q^2+480n^3q+480n^3-120n^2p^3+360n^2pq+730n^2p-120n^2q^3-360n^2q^2+10n^2q+490n^2+60np^4+60np^3+180np^2q+250np^2+180npq^2+760npq+820np+60nq^4+300nq^3+610nq^2+800nq+570n-24p^5-60p^4q-135p^4-120p^3q-160p^3-90p^2q^2-170p^2q-35p^2-60pq^4-360pq^3-710pq^2-430pq+34p-24q^5-195q^4-580q^3-765q^2-396q-40\}$.

3. $W_{ve}(BT_T(n,p,q))=\frac{1}{40}\rho_{MS}\{\gamma_M(360n+86p-194q+520n^2+320n^3+35p^2-110p^3-75p^4-16p^5-425q^2-330q^3-115q^4-16q^5+80np^2+700n^2p-20np^3+320n^3p+40np^4+200nq^2+220n^2q+140nq^3+320n^3q+40nq^4-450pq^2-30p^2q-240pq^3-80p^3q-40pq^4-40p^4q+60n^2p^2-80n^2p^3+80n^3p^2-180n^2q^2-80n^2q^3+80n^3q^2-30p^2q^2+540np+340nq-210pq+400npq+60npq^2+60np^2q+360n^2pq+160n^3pq)+\gamma_S(980+3520n+1062p-518q+3000n^2+960n^3-150p^2-490p^3-170p^4-32p^5-1610q^2-930q^3-250q^4-32q^5+280np^2+2840n^2p-120np^3+800n^3p+80np^4+280nq^2+1640n^2q+200nq^3+800n^3q+80nq^4-1290pq^2-210p^2q-560pq^3-240p^3q-80pq^4-80p^4q+240n^2p^2-160n^2p^3+160n^3p^2-240n^2q^2-160n^2q^3+160n^3q^2-60p^2q^2+3600np+2120nq-500pq+1880npq+120npq^2+120np^2q+1200n^2pq+320n^3pq)\}$.

4. $Sz_v(BT_T(n,p,q))=\frac{1}{120}\rho_{MS}\{\gamma_M^2(120n^3p^3+360n^3p^2q+720n^3p^2+360n^3pq^2+1440n^3pq+1400n^3p+120n^3q^3+720n^3q^2+1400n^3q+880n^3-180n^2p^4-360n^2p^3q-540n^2p^3-360n^2p^2q^2-540n^2p^2q+420n^2p^2-360n^2pq^3-900n^2pq^2+720n^2pq+2100n^2p-180n^2q^4-900n^2q^3-1020n^2q^2+780n^2q+1320n^2+90np^5+90np^4q+180np^3q^2-750np^3+180np^2q^3+360np^2q^2-330np^2q-600np^2+90npq^4-1050npq^2-1320npq+100np+90nq^5+360nq^4-30nq^3-1440nq^2-1340nq-40n-15p^6+45p^5-45p^4q^2-45p^4q+115p^4+90p^3q^2+250p^3q+95p^3-45p^2q^4-90p^2q^3+330p^2q^2+855p^2q+380p^2+45pq^4+250pq^3+585pq^2+700pq+340p-15q^6-45q^5+115q^4+545q^3+620q^2+220q)+\gamma_S^2(480n^3p^3+1440n^3p^2q+4000n^3p^2+1440n^3pq^2+8000n^3pq+10160n^3p+480n^3q^3+4000n^3q^2+10160n^3q+7920n^3-720n^2p^4-1440n^2p^3q-2560n^2p^3-1440n^2p^2q^2-1440n^2p^2q+7560n^2p^2-1440n^2pq^3-2880n^2pq^2+16320n^2pq+33040n^2p-720n^2q^4-4000n^2q^3-120n^2q^2+24160n^2q+27720n^2+360np^5+360np^4q-520np^4+720np^3q^2-1440np^3q-9200np^3+720np^2q^3+720np^2q^2-6000np^2q-6000np^2+360npq^4-1440npq^3-11760npq^2-4640npq+20520np+360nq^5+920nq^4-6960nq^3-22800nq^2-7640nq+16680n-60p^6+424p^5-180p^4q^2+160p^4q+1680p^4+720p^3q^2+1280p^3q-2080p^3-$

$180p^2q^4+3840p^2q^2+5600p^2q-1020p^2+520pq^4+1920pq^3+1280pq^2+2560pq+6816p-60q^6+64q^5+2560q^4+5760q^3+500q^2-2584q+3840)+\gamma_M\gamma_S(480n^3p^3+1440n^3p^2q+3440n^3p^2+1440n^3pq^2+6880n^3pq+7600n^3p+480n^3q^3+3440n^3q^2+7600n^3q+5280n^3-720n^2p^4-1440n^2p^3q-2360n^2p^3-1440n^2p^2q^2-1800n^2p^2q+4320n^2p^2-1440n^2pq^3-3240n^2pq^2+8880n^2pq+18200n^2p-720n^2q^4-3800n^2q^3-2400n^2q^2+11240n^2q+13200n^2+360np^5+360np^4q-260np^4+720np^3q^2-720np^3q-5840np^3+720np^2q^3+1080np^2q^2-3600np^2q-4260np^2+360npq^4-720npq^3-7920npq^2-6760npq+5920np+360nq^5+1180nq^4-3280nq^3-13620nq^2-8640nq+3600n-60p^6+302p^5-180p^4q^2-10p^4q+1030p^4+540p^3q^2+1160p^3q-430p^3-180p^2q^4-180p^2q^3+2580p^2q^2+4870p^2q+1070p^2+350pq^4+1480pq^3+2230pq^2+2820pq+2768p-60q^6-58q^5+1470q^4+4210q^3+2910q^2+48q+600)\}$.

5. $Sz_e(BT_T(n,p,q))=\frac{1}{2}\rho_{MS}^3\{72n^3p^3+216n^3p^2q+408n^3p^2+216n^3pq^2+816n^3pq+772n^3p+72n^3q^3+408n^3q^2+772n^3q+484n^3-108n^2p^4-216n^2p^3q-336n^2p^3-216n^2p^2q^2-432n^2p^2q-42n^2p^2-216n^2pq^3-648n^2pq^2-168n^2pq+564n^2p-108n^2q^4-552n^2q^3-834n^2q^2-144n^2q+342n^2+54np^5+54np^4q+36np^4+108np^3q^2+120np^3q-150np^3+108np^2q^3+336np^2q^2+246np^2q+54npq^4+120npq^3-66npq^2-120npq+166np+54nq^5+252nq^4+306nq^3-72nq^2-170nq+66n-9p^6+15p^5-27p^4q^2-51p^4q+2p^4+18p^3q^2+50p^3q+17p^3-27p^2q^4-90p^2q^3-12p^2q^2+195p^2q+125p^2+3pq^4+26pq^3+117pq^2+214pq+130p-9q^6-39q^5-34q^4+59q^3+107q^2+52q+8\}$.

6. $Sz_{ev}(BT_T(n,p,q))=\frac{1}{20}\rho_{MS}^2\{\gamma_M(40-20n+320p+240q+940n^2+840n^3+350p^2+85p^3+65p^4+35p^5-15p^6+480q^2+355q^3+35q^4-55q^5-15q^6-330np^2+1510n^2p-510np^3+1340n^3p+30np^4+90np^5-820nq^2+270n^2q+230nq^3+1340n^3q+390nq^4+90nq^5+450pq^2+650p^2q+160pq^3+180p^3q+25pq^4-65p^4q+180n^2p^2-550n^2p^3+700n^3p^2-180n^2p^4+120n^3p^3-1200n^2q^2-910n^2q^3+700n^3q^2-180n^2q^4+120n^3q^3+175p^2q^2-120p^2q^3+60p^3q^2-45p^2q^4-45p^4q^2+100np-890nq+615pq-840npq-360n^2p^2q^2-600npq^2+20np^2q+220n^2pq+100npq^3+100np^3q+1400n^3pq+90npq^4+90np^4q+460np^2q^2-990n^2pq^2-630n^2p^2q+180np^2q^3+180np^3q^2-360n^2pq^3-360n^2p^3q+360n^3pq^2+360n^3p^2q)+\gamma_S(610+1120n+1459p+859q+5380n^2+2520n^3+935p^2-60p^3+435p^4+131p^5-30p^6+1855q^2+1920q^3+595q^4-49q^5-30q^6-1660np^2+7400n^2p-2420np^3+3640n^3p-70np^4+180np^5-5560nq^2+4160n^2q-1100nq^3+3640n^3q+650nq^4+180nq^5+1190pq^2+2350p^2q+620pq^3+500p^3q+135pq^4-45p^4q+1620n^2p^2-1200n^2p^3+1680n^3p^2-360n^2p^4+240n^3p^3-1620n^2q^2-1920n^2q^3+1680n^3q^2-360n^2q^4+240n^3q^3+1060p^2q^2-150p^2q^3+210p^3q^2-90p^2q^4-90p^4q^2+1970np-3970nq+1700pq-2920npq-720n^2p^2q^2-3080npq^2-1120np^2q+3240n^2pq-160npq^3-160np^3q+3360n^3pq+180npq^4+180np^4q+740np^2q^2-1800n^2pq^2-1080n^2p^2q+360np^2q^3+360np^3q^2-720n^2pq^3-720n^2p^3q+720n^3pq^2+720n^3p^2q)\}$.

7. $PI(BT_T(n,p,q))=\rho_{MS}^2\{36n^2p^2+72n^2pq+140n^2p+36n^2q^2+140n^2q+140n^2-36np^3-36np^2q-40np^2-36npq^2-16npq+104np-36nq^3-112nq^2-32nq+106n+9p^4-14p^3+18p^2q^2+26p^2q-$

$7p^2 - 10pq^2 - 2pq + 40p + 9q^4 + 22q^3 - 3q^2 - 4q + 42\}$.

8. $S(BT_T(n,p,q)) = \frac{1}{5}\rho_{MS}\{\gamma_M(30 + 300n + 73p - 127q + 380n^2 + 160n^3 - 5p^2 - 70p^3 - 30p^4 - 8p^5 - 235q^2 - 150q^3 - 50q^4 - 8q^5 + 10np^2 + 470n^2p - 40np^3 + 160n^3p + 20np^4 + 10nq^2 + 230n^2q + 40nq^3 + 160n^3q + 20nq^4 - 240pq^2 - 120pq^3 - 40p^3q - 20pq^4 - 20p^4q + 60n^2p^2 - 40n^2p^3 + 40n^3p^2 - 60n^2q^2 - 40n^2q^3 + 40n^3q^2 + 390np + 170nq - 120pq + 200npq + 240n^2pq + 80n^3pq) + \gamma_S(700 + 2360n + 696p - 364q + 1860n^2 + 480n^3 - 180p^2 - 290p^3 - 70p^4 - 16p^5 - 940q^2 - 450q^3 - 110q^4 - 16q^5 + 80np^2 + 1720n^2p - 120np^3 + 400n^3p + 40np^4 - 40nq^2 + 1120n^2q + 40nq^3 + 400n^3q + 40nq^4 - 690pq^2 - 90p^2q - 280pq^3 - 120p^3q - 40pq^4 - 40p^4q + 180n^2p^2 - 80n^2p^3 + 80n^3p^2 - 60n^2q^2 - 80n^2q^3 + 80n^3q^2 + 2280np + 1240nq - 280pq + 1000npq + 720n^2pq + 160n^3pq)\}$.

9. $Gut(BT_T(n,p,q)) = \frac{2}{5}\rho^2_{MS}\{120n^3p^2 + 240n^3pq + 480n^3p + 120n^3q^2 + 480n^3q + 480n^3 - 120n^2p^3 + 180n^2p^2 + 720n^2pq + 1440n^2p - 120n^2q^3 - 180n^2q^2 + 720n^2q + 1200n^2 + 60np^4 - 120np^3 + 60np^2 + 720npq + 1440np + 60nq^4 + 120nq^3 + 60nq^2 + 720nq + 1195n - 24p^5 - 60p^4q - 90p^4 - 120p^3q - 240p^3 - 60p^2q - 120p^2 - 60pq^4 - 360pq^3 - 780pq^2 - 480pq + 224p - 24q^5 - 150q^4 - 480q^3 - 840q^2 - 496q + 155\}$.

Table 3: Strength-weighted parameters of $BT_T(n,p,q)/X_i^{Tb}$, $X \in \{H, O, A, P\}$

Θ-class	Edge-strength $X_{3i}^{Tb}(s)$	Vertex weight $X_{1i}^{Tb}(w)$	Vertex strength $X_{1i}^{Tb}(s)$
H_i^{Tb}:$1 \le i \le q+1$	$\rho_{MS}(2i + 2n - 2q - 1)$	$(\gamma_S(2i + 2n - 2q + 2i^2 + 4ni - 4iq) + \gamma_M(i^2 - i + 2ni - 2iq))/2$	$\rho_{MS}(q - n - 4i + 6ni - 6iq + 3i^2 + 1)$
H_{-i}^{Tb}:$1 \le i \le p$	$\rho_{MS}(2i + 2n - 2p + 1)$	$(\gamma_S(2 + 6i + 2n - 2p + 2i^2 + 4ni - 4ip) + \gamma_M(i + i^2 + 2ni - 2ip))/2$	$\rho_{MS}(2i - n + p + 6ni - 6ip + 3i^2)$
A_i^{Tb}:$1 \le i \le p$	$\rho_{MS}(2i + 2q + 3)$	$(\gamma_S(4 + 10i + 2q + 2i^2 + 4iq) + \gamma_M(3i + i^2 + 2iq))/2$	$\rho_{MS}(8i - q + 6iq + 3i^2 - 1)$
A_i^{Tb}:$p+1 \le i \le n-q-1$	$2\rho_{MS}(p + q + 2)$	$(\gamma_S(4 + 12i - 2p + 2q - 2p^2 + 4ip + 4iq) + \gamma_M(4i - p - p^2 + 2ip + 2iq))/2$	$\rho_{MS}(12i - 4p - q + 6ip + 6iq - 3p^2 - 2)$
A_{-i}^{Tb}:$1 \le i \le q+1$	$\rho_{MS}(2i + 2p + 1)$	$\gamma_S(p + 1 + i(i + 2p + 3)) + i\gamma_M(i + 2p + 1)/2$	$\rho_{MS}(2i - p + 6ip + 3i^2)$
P_i^{Tb}:$1 \le i \le 2n + p + q + 7$	ρ_{MS}	γ_S	0

Proof. The cardinality of the structural vertex and edge sets of $BT_T(n,p,q)$ are given as $|V_\gamma(BT_T(n,p,q))|$

$= (\gamma_M(2+4n+p-q-p^2-q^2+2np+2nq)+\gamma_S(14+12n+4p-2p^2-2q^2+4np+4nq))/2$ and $|E_\rho(BT_T(n,p,q))| = 3\rho_{MS}(4n+p-q+2np+2nq-p^2-q^2+2)$ and which contains $(16n+5p-q+6np+6nq-3p^2-3q^2+16)/2$ vertices and $3(4n+p-q+2np+2nq-p^2-q^2+2)$ edges in the underlying graph.

The strength-weighted parameters of the quotient graphs for various Θ-partitions are listed in Table 3 with $X^{Tb}_{2i}(w) = |V_\gamma(BT_T(n,p,q))| - X^{Tb}_{1i}(w)$ and $X^{Tb}_{2i}(s) = |E_\rho(BT_T(n,p,q))| - X^{Tb}_{1i}(s) - X^{Tb}_{3i}(s)$. Thus we now compute the various indices $TI \in \{W, W_e, W_{ve}, Sz_v, Sz_e, Sz_{ev}, PI, S, Gut\}$ using the expression,

$$\begin{aligned} TI(BT_T(n,p,q)) =& \sum_{i=1}^{q+1} TI(BT_T(n,p,q)/H^{Tb}_i) + \sum_{i=1}^{p} TI(BT_T(n,p,q)/H^{Tb}_{-i}) \\ &+ 2\sum_{i=1}^{p} TI(BT_T(n,p,q)/A^{Tb}_i) + 2\sum_{i=p+1}^{n-q-1} TI(BT_T(n,p,q)/A^{Tb}_i) \\ &+ 2\sum_{i=1}^{q+1} TI(BT_T(n,p,q)/A^{Tb}_{-i}) + \sum_{i=1}^{2n+p+q+7} TI(BT_T(n,p,q)/P^{Tb}_i). \end{aligned}$$

□

Theorem 8. *For $p+q=n$, let $BT_T(n,p,q) = BT_T(n,p)$ be a 1T MS_2 monolayer. Then*

1. $W(BT_T(n,p)) = \frac{1}{60}\{\gamma_M^2(6n^5+30n^4p+45n^4+160n^3p+120n^3-60n^2p^3-30n^2p^2+300n^2p+135n^2+30np^4-140np^3-60np^2+250np+54n+40p^4-80p^3-40p^2+80p)+\gamma_S^2(24n^5+120n^4p+360n^4+1120n^3p+2000n^3-240n^2p^3-480n^2p^2+3540n^2p+5340n^2+120np^4-800np^3-1860np^2+4240np+6676n+280p^4-560p^3-1420p^2+1700p+3120)+\gamma_M\gamma_S(24n^5+120n^4p+270n^4+880n^3p+1090n^3-240n^2p^3-300n^2p^2+2280n^2p+2010n^2+120np^4-680np^3-960np^2+2500np+1706n+220p^4-440p^3-760p^2+980p+540)\}$.

2. $W_e(BT_T(n,p)) = \frac{1}{10}\rho_{MS}^2\{36n^5+180n^4p+225n^4+780n^3p+520n^3-360n^2p^3-180n^2p^2+1290n^2p+525n^2+180np^4-480np^3-390np^2+1120np+174n+60p^4-120p^3-370p^2+430p-20\}$.

3. $W_{ve}(BT_T(n,p)) = \frac{1}{40}\rho_{MS}\{\gamma_M(166n+280p+435n^2+410n^3+165n^4+24n^5-180p^2-200p^3+100p^4-240np^2+1020n^2p-440np^3+580n^3p+120np^4+120n^4p-120n^2p^2-240n^2p^3+840np)+\gamma_S(980+3002n+1580p+3510n^2+1950n^3+510n^4+48n^5-1260p^2-640p^3+320p^4-1740np^2+4020n^2p-1120np^3+1640n^3p+240np^4+240n^4p-600n^2p^2-480n^2p^3+4200np)\}$.

4. $Sz_v(BT_T(n,p)) = \frac{1}{120}\rho_{MS}\{\gamma_M^2(15n^6+90n^5p+135n^5+90n^4p^2+630n^4p+465n^4-240n^3p^3+360n^3p^2+1590n^3p+765n^3-180n^2p^4-1080n^2p^3+630n^2p^2+1830n^2p+600n^2+360np^5-180np^4-1560np^3+600np^2+900np+180n-120p^6+360p^5+60p^4-720p^3+300p^2+120p)+\gamma_S^2(60n^6+360n^5p+984n^5+360n^4p^2+4200n^4p+5640n^4-960n^3p^3+1440n^3p^2+17360n^3p+$

$15040n^3-720n^2p^4-7680n^2p^3+1200n^2p^2+33840n^2p+20580n^2+1440np^5+960np^4-18880np^3-3840np^2+29720np+14096n-480p^6+1440p^5+4880p^4-12160p^3-3080p^2+9400p+3840)+\gamma_M\gamma_S(60n^6+360n^5p+762n^5+360n^4p^2+3360n^4p+3390n^4-960n^3p^3+1440n^3p^2+11200n^3p+7110n^3-720n^2p^4-6000n^2p^3+2400n^2p^2+17040n^2p+7470n^2+1440np^5+120np^4-12320np^3+1920np^2+11560np+3648n-480p^6+1440p^5+2440p^4-7280p^3+1160p^2+2720p+600)\}$.

5. $Sz_e(BT_T(n,p))=\frac{1}{2}\rho_{MS}^3\{9n^6+54n^5p+69n^5+54n^4p^2+318n^4p+210n^4-144n^3p^3+204n^3p^2+678n^3p+327n^3-108n^2p^4-504n^2p^3+294n^2p^2+672n^2p+267n^2+216np^5-180np^4-480np^3+186np^2+312np+98n-72p^6+216p^5-120p^4-120p^3+42p^2+54p+8\}$.

6. $Sz_{ev}(BT_T(n,p))=\frac{1}{20}\rho_{MS}^2\{\gamma_M(20+190n+60p+520n^2+645n^3+405n^4+125n^5+15n^6+235p^2-470p^3-65p^4+360p^5-120p^6+505np^2+1425n^2p-1190np^3+1350n^3p-240np^4+580n^4p+360np^5+90n^5p+575n^2p^2-960n^2p^3+350n^3p^2-180n^2p^4-240n^3p^3+90n^4p^2+625np)+\gamma_S(470+1859n+560p+3245n^2+3040n^3+1515n^4+361n^5+30n^6+1130p^2-3140p^3+970p^4+720p^5-240p^6+1430np^2+6870n^2p-5420np^3+4940n^3p-60np^4+1580n^4p+720np^5+180n^5p+1270n^2p^2-2760n^2p^3+700n^3p^2-360n^2p^4-480n^3p^3+180n^4p^2+3890np)\}$.

7. $PI(BT_T(n,p))=\rho_{MS}^2\{9n^4+36n^3p+50n^3+132n^2p+105n^2-72np^3-24np^2+140np+102n+36p^4-72p^3-8p^2+44p+38\}$.

8. $S(BT_T(n,p))=\frac{1}{5}\rho_{MS}\{\gamma_M(30+173n+200p+315n^2+250n^3+90n^4+12n^5-120p^2-160p^3+80p^4-150np^2+630n^2p-280np^3+320n^3p+60np^4+60n^4p-60n^2p^2-120n^2p^3+570np)+\gamma_S(700+1996n+1060p+2160n^2+1110n^3+270n^4+24n^5-840p^2-440p^3+220p^4-1020np^2+2340n^2p-680np^3+880n^3p+120np^4+120n^4p-300n^2p^2-240n^2p^3+2640np)\}$.

9. $Gut(BT_T(n,p))=\frac{6}{5}\rho_{MS}^2\{12n^5+60n^4p+90n^4+320n^3p+260n^3-120n^2p^3-60n^2p^2+660n^2p+360n^2+60np^4-280np^3-180np^2+640np+233n+80p^4-160p^3-160p^2+240p+55\}$.

Proof. In this case, we have the same strength-weight parameter values as in Table 3 for all Θ-classes except for the Θ-class A_p^{Tb}, where we have $A_{3p}^{Tb}(s)=\rho_{MS}(i+p+2q+2)$. The parameter set $\{n,p,q\}$ also reduces to $\{n,p,n-p\}$. Thus following the proof lines of Theorem 7, we obtain the desired results using the following expression:

$$\begin{aligned}TI(BT_T(n,p))=&\sum_{i=1}^{q+1}TI(BT_T(n,p)/H_i^{Tb})+\sum_{i=1}^{p}TI(BT_T(n,p)/H_{-i}^{Tb})\\&+2\sum_{i=1}^{p-1}TI(BT_T(n,p)/A_i^{Tb})+2TI(BT_T(n,p)/A_p^{Tb})\\&+2\sum_{i=1}^{q}TI(BT_T(n,p)/A_{-i}^{Tb})+\sum_{i=1}^{2n+p+q+7}TI(BT_T(n,p)/P_i^{Tb}).\end{aligned}$$

□

Since $H_j(k) = BT_j(2k-1, k-1, k-1)$ and consequently, all the indices namely $W, W_e, W_{ev}, Sz_v, Sz_e, Sz_{ev}, PI, S, Gut$ for this structure can be obtained from Theorems 6 and 7 by replacing the values of the parameters n, p and q as $2k-1$, $k-1$ and $k-1$ respectively.

In order to compute the indices $TI \in \{Mo, Mo_e, Mo_t, w^+Mo, w^+Mo_e, w^+Mo_t, w^*Mo, w^*Mo_e, w^*Mo_t\}$, it is sufficient to estimate the edge-weight parameters for the Θ-classes H_i^{jh} and P_i^{jh} owing to the symmetry of the structure. For $H_H(k)$, we have $H_{\pm 3i}^{Hh}(w^+) = \rho_{MS}(6(k+i)-2)$, $H_{\pm 3i}^{Hh}(w^*) = \rho_{MS}^2(9(k+i)-6)$, $P_{3i}^{Hh}(w^+) = 4\rho_{MS}$ and $P_{3i}^{Hh}(w^*) = 3\rho_{MS}^2$. Analogously for $H_T(k)$, we obtain the edge-weight parameters as, $H_{3i}^{Th}(w^+) = \rho_{MS}(18(i+k)-11)$, $H_{3i}^{Th}(w^*) = 6\rho_{MS}^2(6(i+k)-5)$, $H_{-3i}^{Th}(w^+) = \rho_{MS}(18(i+k)+7)$, $H_{-3i}^{Th}(w^*) = 6\rho_{MS}^2(6(i+k)+1)$, $P_{3i}^{Th}(w^+) = 7\rho_{MS}$ and $P_{3i}^{Th}(w^*) = 6\rho_{MS}^2$.

Theorem 9. *For parallelogram shape 2H MS_2 monolayer $P_H(p,q)$, $1 \le q \le p$, we have*

1. $W(P_H(p,q)) = \frac{1}{60}\{\gamma_M^2(20p^3q^2+40p^3q+20p^3+10p^2q^3+90p^2q^2+140p^2q+60p^2+5pq^4+40pq^3+125pq^2+130pq+40p-q^5+25q^3+60q^2+36q)+\gamma_S^2(20p^3q^2+80p^3q+80p^3+10p^2q^3+180p^2q^2+530p^2q+480p^2+5pq^4+80pq^3+515pq^2+1100pq+760p-q^5+85q^3+480q^2+756q+360)+\gamma_M\gamma_S(40p^3q^2+120p^3q+80p^3+20p^2q^3+270p^2q^2+610p^2q+360p^2+10pq^4+120pq^3+580pq^2+930pq+460p-2q^5+90q^3+360q^2+452q+180)\}$.

2. $W_e(P_H(p,q)) = \frac{1}{20}\rho_{MS}^2(q+1)\{60p^3q+60p^3+30p^2q^2+150p^2q+120p^2+15pq^3+105pq^2+150pq+60p-3q^4+3q^3+62q^2+58q\}$.

3. $W_{ev}(P_H(p,q)) = \frac{1}{60}\rho_{MS}\{\gamma_M(90p+83q+150p^2+60p^3+150q^2+70q^3-3q^5+315pq^2+345p^2q+120pq^3+120p^3q+15pq^4+225p^2q^2+30p^2q^3+60p^3q^2+300pq)+\gamma_S(180+540p+533q+480p^2+120p^3+480q^2+130q^3-3q^5+750pq^2+780p^2q+180pq^3+180p^3q+15pq^4+360p^2q^2+30p^2q^3+60p^3q^2+1095pq)\}$.

4. $Sz_v(P_H(p,q)) = \frac{1}{60}\rho_{MS}\{\gamma_M^2(30p^3q^3+90p^3q^2+80p^3q+20p^3+90p^2q^3+270p^2q^2+240p^2q+60p^2+70pq^3+210pq^2+180pq+40p+5q^4+30q^3+55q^2+30q)+\gamma_S^2(30p^3q^3+160p^3q^2+210p^3q+80p^3+170p^2q^3+810p^2q^2+1060p^2q+480p^2-5pq^4+200pq^3+1045pq^2+1540pq+760p+q^5+5q^4+85q^3+475q^2+754q+360)+\gamma_M\gamma_S(60p^3q^3+250p^3q^2+270p^3q+80p^3+260p^2q^3+990p^2q^2+1090p^2q+360p^2-5pq^4+250pq^3+1045pq^2+1250pq+460p+q^5+10q^4+95q^3+350q^2+444q+180)\}$.

5. $Sz_e(P_H(p,q)) = \frac{1}{2}\rho_{MS}^3(q+1)^2(p+1)\{9p^2q+6p^2+12pq+6p+q^2+5q\}$.

6. $Sz_{ev}(P_H(p,q)) = \frac{1}{120}\rho_{MS}^2\{\gamma_M(180p+140q+300p^2+120p^3+275q^2+160q^3+25q^4+1040pq^2+1170p^2q+400pq^3+450p^3q+10pq^4+1350p^2q^2+480p^2q^3+510p^3q^2+180p^3q^3+830pq)+\gamma_S(360+1080p+1032q+960p^2+240p^3+925q^2+285q^3+35q^4+3q^5+2525pq^2+2670p^2q+650pq^3+720p^3q-5pq^4+2610p^2q^2+720p^2q^3+720p^3q^2+180p^3q^3+2830pq)\}$.

7. $PI(P_H(p,q)) = \frac{1}{3}\rho_{MS}^2\{27p^2q^2 + 51p^2q + 27p^2 + 48pq^2 + 90pq + 45p + q^3 + 27q^2 + 44q + 18\}$.

8. $S(P_H(p,q)) = \frac{1}{15}\rho_{MS}\{\gamma_M(45+180p+173q+195p^2+60p^3+195q^2+70q^3-3q^5+405pq^2+435p^2q+120pq^3+120p^3q+15pq^4+270p^2q^2+30p^2q^3+60p^3q^2+480pq)+\gamma_S(315+765p+758q+570p^2+120p^3+570q^2+130q^3-3q^5+885pq^2+915p^2q+180pq^3+180p^3q+15pq^4+405p^2q^2+30p^2q^3+60p^3q^2+1455pq)\}$.

9. $Gut(P_H(p,q)) = \frac{1}{15}\rho_{MS}^2\{180p^3q^2+360p^3q+180p^3+90p^2q^3+810p^2q^2+1335p^2q+630p^2+45pq^4+360pq^3+1275pq^2+1620pq+675p-9q^5+200q^3+630q^2+664q+225\}$.

10. $Mo(P_H(p,q)) = \frac{1}{24}\rho_{MS}\{\gamma_M(54+84p+96q+42p^2+48q^2+72pq^2+72p^2q+36p^2q^2+144pq+6(-1)^p(q+1)^2+6(-1)^q(p+1)^2+6(-1)^{p+q}(q+1)^2)+z(72+174p+176q+102p^2+108q^2+4q^3+84pq^2+96p^2q+36p^2q^2+216pq-6(-1)^pq(q+1)-6(-1)^qp(p+1)+6(-1)^{p+q}q(q+1))\}$.

11. $Mo_e(P_H(p,q)) = \frac{1}{8}\rho_{MS}^2\{84p+88q+144pq+72pq^2+72p^2q+46p^2+48q^2+36p^2q^2+42+2(-1)^p(q+1)^2+2(-1)^q(p+1)^2+2(-1)^{p+q}(q+1)^2\}$.

12. $Mo_t(P_H(p,q)) = \frac{1}{24}\rho_{MS}\{\rho_{MS}(126+252p+264q+138p^2+144q^2+216pq^2+216p^2q+108p^2q^2+432pq+6(-1)^p(q+1)^2+6(-1)^q(p+1)^2+6(-1)^{p+q}(q+1)^2)+\gamma_M(54+84p+96q+42p^2+48q^2+72pq^2+72p^2q+36p^2q^2+144pq+6(-1)^p(q+1)^2+6(-1)^q(p+1)^2+6(-1)^{p+q}(q+1)^2)+\gamma_S(72+174p+176q+102p^2+108q^2+4q^3+84pq^2+96p^2q+36p^2q^2+216pq-6(-1)^pq(q+1)-6(-1)^qp(p+1)+6(-1)^{p+q}q(q+1))\}$.

13. $w^+Mo(P_H(p,q)) = \frac{1}{120}\rho_{MS}^2\{\gamma_M(990+1440p+1808q+570p^2-180p^3+960q^2+40q^3+120q^4+72q^5+2160pq^2+2400p^2q-240pq^3-240pq^4+3060p^2q^2+720p^2q^3+360p^3q^2+3120pq+30(-1)^p(6q+5)(q+1)^2+30(-1)^q(6p+5)(p+1)^2+30(-1)^{p+q}(6q+5)(q+1)^2)+\gamma_S(1440+3510p+3568q+2490p^2+180p^3+2700q^2+620q^3+240q^4+72q^5+2820pq^2+3720p^2q-480pq^3-240pq^4+4140p^2q^2+720p^2q^3+360p^3q^2+4800pq-30(-1)^pq(6q+5)(q+1)-30(-1)^qp(6p+5)(p+1)+30(-1)^{p+q}q(6q+5)(q+1))\}$.

14. $w^+Mo_e(P_H(p,q)) = \frac{1}{120}\rho_{MS}^3\{4800p+5224q+9360pq+6480pq^2+7200p^2q-720pq^3-720pq^4+2730p^2-180p^3+3120q^2+200q^3+360q^4+216q^5+9180p^2q^2+2160p^2q^3+1080p^3q^2+2430+30(-1)^p(6q+5)(q+1)^2+30(-1)^q(6p+5)(p+1)^2+30(-1)^{p+q}(6q+5)(q+1)^2\}$.

15. $w^+Mo_t(P_H(p,q)) = \frac{1}{120}\rho_{MS}^2\{\gamma_M(990+1440p+1808q+570p^2-180p^3+960q^2+40q^3+120q^4+72q^5+2160pq^2+2400p^2q-240pq^3-240pq^4+720p^2q^3+360p^3q^2+3060p^2q^2+3120pq+30(-1)^p(6q+5)(q+1)^2+30(-1)^q(6p+5)(p+1)^2+30(-1)^{p+q}(6q+5)(q+1)^2)+\rho_{MS}(2430+4800p+5224q+2730p^2-180p^3+3120q^2+200q^3+360q^4+216q^5+6480pq^2+7200p^2q-720pq^3-720pq^4+9180p^2q^2+2160p^2q^3+1080p^3q^2+9360pq+30(-1)^p(6q+5)(q+1)^2+30(-1)^q(6p+5)(p+1)^2+30(-1)^{p+q}(6q+5)(q+1)^2)+\gamma_S(1440+3510p+3568q+2490p^2+180p^3+2700q^2+620q^3+$

$240q^4+72q^5+2820pq^2+3720p^2q-480pq^3-240pq^4+4140p^2q^2+720p^2q^3+360p^3q^2+4800pq-30(-1)^pq(6q+5)(q+1)-30(-1)^qp(6p+5)(p+1)+30(-1)^{p+q}q(6q+5)(q+1))\}$.

16. $w^*Mo(P_H(p,q))=\frac{1}{40}\rho_{MS}^3\{\gamma_M(180+270p+404q+120p^2-90p^3+300q^2+60q^4+36q^5+40q^3+780pq^2+960p^2q-120pq^3-120pq^4+1440p^2q^2+360p^2q^3+180p^3q^2+840pq+30(-1)^p(3q+2)(q+1)^2+30(-1)^q(3p+2)(p+1)^2+30(-1)^{p+q}(3q+2)(q+1)^2)+\gamma_S(360+900p+1024q+870p^2+90p^3+1020q^2+320q^3+120q^4+36q^5+1080pq^2+1560p^2q-240pq^3-120pq^4+1980p^2q^2+360p^2q^3+180p^3q^2+1320pq-30(-1)^pq(q+1)(3q+2)-30(-1)^qp(p+1)(3p+2)+30(-1)^{p+q}q(q+1)(3q+2))\}$.

17. $w^*Mo_e(P_H(p,q))=\frac{1}{40}\rho_{MS}^4\{1110p+1372q+2520pq+2340pq^2+2880p^2q-360pq^3-360pq^4+840p^2-90p^3+1140q^2+200q^3+180q^4+108q^5+4320p^2q^2+1080p^2q^3+540p^3q^2+540+30(-1)^p(3q+2)(q+1)^2+30(-1)^q(3p+2)(p+1)^2+30(-1)^{p+q}(3q+2)(q+1)^2\}$.

18. $w^*Mo_t(P_H(p,q))=\frac{1}{40}\rho_{MS}^3\{\rho_{MS}(540+1110p+1372q+840p^2-90p^3+1140q^2+200q^3+180q^4+108q^5-360pq^3-360pq^4+4320p^2q^2+1080p^2q^3+540p^3q^2+2520pq+2340pq^2+2880p^2q+30(-1)^p(3q+2)(q+1)^2+30(-1)^q(3p+2)(p+1)^2+30(-1)^{p+q}(3q+2)(q+1)^2)+\gamma_M(180+270p+404q+120p^2-90p^3+300q^2+40q^3+60q^4+36q^5+780pq^2+960p^2q-120pq^3-120pq^4+1440p^2q^2+360p^2q^3+180p^3q^2+840pq+30(-1)^p(3q+2)(q+1)^2+30(-1)^q(3p+2)(p+1)^2+30(-1)^{p+q}(3q+2)(q+1)^2)+\gamma_S(360+900p+1024q+870p^2+90p^3+1020q^2+320q^3+120q^4+36q^5+1080pq^2+1560p^2q-240pq^3-120pq^4+1980p^2q^2+360p^2q^3+180p^3q^2+1320pq-30(-1)^pq(q+1)(3q+2)-30(-1)^qp(p+1)(3p+2)+30(-1)^{p+q}q(q+1)(3q+2))\}$.

Proof. The monolayer $P_H(p,q)$ contains $3(p+q)+2(pq+2)$ number of vertices and $3(p+1)(q+1)$ number of edges with $|V_\gamma(P_H(p,q))|=\gamma_M(1+p+q+pq)+\gamma_S(3+2p+2q+pq)$ and $|E_\rho(P_H(p,q))|=3\rho_{MS}(p+1)(q+1)$. The strength-weighted parameters of the various quotient graphs corresponding to the Θ-classes of $P_H(p,q)$ are tabulated in Table 4. Obviously, $X_{2i}^{Hp}(w)=|V_\gamma(P_H(p,q))|-X_{1i}^{Hp}(w)$ and $X_{2i}^{Hp}(s)=|E_\rho(P_H(p,q))|-X_{1i}^{Hp}(s)-X_{3i}^{Hp}(s)$.

We therefore derive the indices $TI\in\{W,W_e,W_{ev},Sz_v,Sz_e,Sz_{ev},PI,S,Gut,Mo,Mo_e,Mo_t,w^+Mo,w^+Mo_e,w^+Mo_t,w^*Mo,w^*Mo_e,w^*Mo_t\}$ through the expression

$$\begin{aligned}TI(P_H(p,q))=&\sum_{i=1}^{q}TI(P_H(p,q)/H_i^{Hp})+\sum_{i=1}^{p}TI(P_H(p,q)/O_i^{Hp})+\sum_{i=1}^{q}TI(P_H(p,q)/A_i^{Hp})+\\&+\sum_{i=q+1}^{p}TI(P_H(p,q)/A_i^{Hp})+\sum_{i=1}^{q}TI(P_H(p,q)/A_{-i}^{Hp})+\sum_{i=1}^{p+q+3}TI(P_H(p,q)/P_i^{Hp}).\end{aligned}$$

Table 4: Strength-weighted parameters of the quotient graphs $P_H(p,q)/X_{ki}^{Hp}$, $X \in \{H, O, A, P\}$

Θ-class	Vertex parameters (w_v, s_v)	Edge parameters ($w_e^*/w_e^+, s_e$)
H_i^{Hp}:$1 \le i \le q$	$H_{1i}^{Hp}(w) = i\gamma_S(2+p) + i\gamma_M(1+p)$	$H_{3i}^{Hp}(s) = \rho_{MS}(p+1)$
		$H_{3i}^{Hp}(w^+) = \rho_{MS}(6p+5)$
	$H_{1i}^{Hp}(s) = \rho_{MS}(3i-1)(p+1)$	$H_{3i}^{Hp}(w^*) = \rho_{MS}^2(9p+6)$
O_i^{Hp}:$1 \le i \le p$	$O_{1i}^{Hp}(w) = \gamma_S(2i+q+iq+1)$ $+i\gamma_M(q+1)$	$O_{3i}^{Hp}(s) = \rho_{MS}(q+1)$
		$O_{3i}^{Hp}(w^+) = \rho_{MS}(6q+5)$
	$O_{1i}^{Hp}(s) = 3i\rho_{MS}(q+1)$	$O_{3i}^{Hp}(w^*) = \rho_{MS}^2(9q+6)$
A_i^{Hp}:$1 \le i \le q$	$A_{1i}^{Hp}(w) = i(\gamma_M(1+i) + \gamma_S(3+i))/2$	$A_{3i}^{Hp}(s) = i\rho_{MS}$
		$A_{3i}^{Hp}(w^+) = 6i\rho_{MS}$
	$A_{1i}^{Hp}(s) = i\rho_{MS}(3i+1)/2$	$A_{3i}^{Hp}(w^*) = 9i\rho_{MS}^2$
A_i^{Hp}:$q+1 \le i \le p$	$A_{1i}^{Hp}(w) = (\gamma_M(2i-q-q^2+2iq)$ $+\gamma_S(4i-q-q^2+2iq))/2$	$A_{3i}^{Hp}(s) = \rho_{MS}(q+1)$
		$A_{3i}^{Hp}(w^+) = \rho_{MS}(6q+5)$
	$A_{1i}^{Hp}(s) = \rho_{MS}(q+1)(6i-3q-2)/2$	$A_{3i}^{Hp}(w^*) = \rho_{MS}^2(9q+6)$
A_{-i}^{Hp}:$1 \le i \le q$	$A_{-1i}^{Hp}(w) = (i+1)(i\gamma_M + (i+2)\gamma_S)/2$	$A_{-3i}^{Hp}(s) = \rho_{MS}(i+1)$
		$A_{-3i}^{Hp}(w^+) = \rho_{MS}(6i+4)$
	$A_{-1i}^{Hp}(s) = 3i\rho_{MS}(i+1)/2$	$A_{-3i}^{Hp}(w^*) = \rho_{MS}^2(9i+3)$
P_i^{Hp}:$1 \le i \le p+q+3$	$P_{1i}^{Hp}(w) = \gamma_S$	$P_{3i}^{Hp}(s) = \rho_{MS}$
		$P_{3i}^{Hp}(w^+) = 4\rho_{MS}$
	$P_{1i}^{Hp}(s) = 0$	$P_{3i}^{Hp}(w^*) = 3\rho_{MS}^2$

□

Theorem 10. *For parallelogram shape 1T MS_2 monolayer $P_T(p,q)$, $1 \le q \le p$, we have*

1. $W(P_T(p,q)) = \frac{1}{60}\{y^2(20p^3q^2+40p^3q+20p^3+10p^2q^3+90p^2q^2+140p^2q+60p^2+5pq^4+40pq^3+125pq^2+130pq+40p-q^5+25q^3+60q^2+36q)+\gamma_S^2(80p^3q^2+320p^3q+320p^3+40p^2q^3+720p^2q^2+2180p^2q+1920p^2+20pq^4+320pq^3+2120pq^2+4640pq+3280p-4q^5+340q^3+1920q^2+3264q+1800)+y\gamma_S(80p^3q^2+240p^3q+160p^3+40p^2q^3+540p^2q^2+1220p^2q+720p^2+20pq^4+240pq^3+1160pq^2+1860pq+920p-4q^5+180q^3+720q^2+904q+360)\}$.

2. $W_e(P_T(p,q)) = \frac{1}{15}\rho_{MS}^2\{180p^3q^2+360p^3q+180p^3+90p^2q^3+540p^2q^2+825p^2q+360p^2+45pq^4+360pq^3+795pq^2+720pq+210p-9q^5+190q^3+360q^2+194q\}$.

3. $W_{ve}(P_T(p,q)) = \frac{1}{30}\rho_{MS}\{y(90p+83q+150p^2+60p^3+150q^2+70q^3-3q^5+315pq^2+345p^2q+120pq^3+120p^3q+15pq^4+225p^2q^2+30p^2q^3+60p^3q^2+300pq)+\gamma_S(450+1170p+1156q+960p^2+240p^3+960q^2+260q^3-6q^5+1530pq^2+1590p^2q+360pq^3+360p^3q+30pq^4+720p^2q^2+60p^2q^3+120p^3q^2+2340pq)\}$.

4. $Sz_v(P_T(p,q)) = \frac{1}{30}\rho_{MS}\{\gamma_M^2(30p^3q^3+90p^3q^2+80p^3q+20p^3+90p^2q^3+270p^2q^2+240p^2q+60p^2+70pq^3+210pq^2+180pq+40p+5q^4+30q^3+55q^2+30q)+\gamma_S^2(120p^3q^3+640p^3q^2+900p^3q+320p^3+680p^2q^3+3240p^2q^2+4300p^2q+1680p^2-20pq^4+860pq^3+4120pq^2+5500pq+2260p+4q^5+20q^4+380q^3+1660q^2+2196q+900)+\gamma_M\gamma_S(120p^3q^3+500p^3q^2+540p^3q+160p^3+520p^2q^3+1980p^2q^2+2120p^2q+660p^2-10pq^4+500pq^3+1970pq^2+2140pq+680p+2q^5+20q^4+210q^3+640q^2+628q+180)\}$.

5. $Sz_e(P_T(p,q)) = 2\rho_{MS}^3\{18p^3q^3+48p^3q^2+43p^3q+12p^3+42p^2q^3+108p^2q^2+93p^2q+24p^2+2pq^4+37pq^3+82pq^2+64pq+14p+3q^4+16q^3+23q^2+11q\}$.

6. $Sz_{ev}(P_T(p,q)) = \frac{1}{60}\rho_{MS}^2\{\gamma_M(360p+280q+600p^2+240p^3+565q^2+350q^3+65q^4+2020pq^2+2340p^2q+770pq^3+900p^3q+20pq^4+2700p^2q^2+960p^2q^3+1020p^3q^2+360p^3q^3+1630pq)+\gamma_S(900+3300p+3128q+3480p^2+960p^3+3430q^2+1300q^3+170q^4+12q^5+9680pq^2+10680p^2q+2660pq^3+3000p^3q-20pq^4+10440p^2q^2+2880p^2q^3+2880p^3q^2+720p^3q^3+10000pq)\}$.

7. $PI(P_T(p,q)) = \frac{2}{3}\rho_{MS}^2\{54p^2q^2+102p^2q+54p^2+96pq^2+180pq+93p+2q^3+54q^2+94q+45\}$.

8. $S(P_T(p,q)) = \frac{2}{15}\rho_{MS}\{\gamma_M(45+180p+173q+195p^2+60p^3+195q^2+70q^3-3q^5+405pq^2+435p^2q+120pq^3+120p^3q+15pq^4+270p^2q^2+30p^2q^3+60p^3q^2+480pq)+\gamma_S(720+1620p+1606q+1140p^2+240p^3+1140q^2+260q^3-6q^5+1800pq^2+1860p^2q+360pq^3+360p^3q+30pq^4+810p^2q^2+60p^2q^3+120p^3q^2+3060pq)\}$.

9. $Gut(P_T(p,q)) = \frac{2}{5}\rho_{MS}^2\{120p^3q^2+240p^3q+120p^3+60p^2q^3+540p^2q^2+900p^2q+420p^2+30pq^4+240pq^3+870pq^2+1140pq+475p-6q^5+130q^3+420q^2+466q+165\}$.

10. $Mo(P_T(p,q)) = \frac{1}{12}\rho_{MS}\{\gamma_M(54+84p+96q+42p^2+48q^2+72pq^2+72p^2q+36p^2q^2+144pq+6(-1)^p(q+1)^2+6(-1)^q(p+1)^2+6(-1)^{p+q}(q+1)^2)+\gamma_S(216+348p+376q+180p^2+192q^2+8q^3+168pq^2+192p^2q+72p^2q^2+432pq+12(-1)^p(q+2)(q+1)+12(-1)^q(p+2)(p+1)+12(-1)^{p+q}(q+2)(q+1))\}$.

11. $Mo_e(P_T(p,q)) = \frac{1}{2}\rho_{MS}^2\{80p+84q+144pq+72pq^2+72p^2q+42p^2+44q^2+36p^2q^2+42+6(-1)^p(q+1)^2+6(-1)^q(p+1)^2+6(-1)^{p+q}(q+1)^2\}$.

12. $Mo_t(P_T(p,q)) = \frac{1}{12}\rho_{MS}\{\rho_{MS}(252+480p+504q+252p^2+264q^2+432pq^2+432p^2q+216p^2q^2+864pq+36(-1)^p(q+1)^2+36(-1)^q(p+1)^2+36(-1)^{p+q}(q+1)^2)+\gamma_M(54+84p+96q+42p^2+$

$48q^2 + 72pq^2 + 72p^2q + 36p^2q^2 + 144pq + 6(-1)^p(q+1)^2 + 6(-1)^q(p+1)^2 + 6(-1)^{p+q}(q+1)^2) + \gamma_S(216 + 348p + 376q + 180p^2 + 192q^2 + 8q^3 + 168pq^2 + 192p^2q + 72p^2q^2 + 432pq + 12(-1)^p(q+2)(q+1) + 12(-1)^q(p+2)(p+1) + 12(-1)^{p+q}(q+2)(q+1))\}$.

13. $w^+Mo(P_T(p,q)) = \frac{1}{30}\rho_{MS}^2\{\gamma_M(540+930p+1392q+600p^2-270p^3+1200q^2+180q^3+180q^4+108q^5+2700pq^2+3420p^2q-360pq^3-360pq^4+4680p^2q^2+1080p^2q^3+540p^3q^2+2880pq+30(-1)^p(9q+8)(q+1)^2+30(-1)^q(9p+8)(p+1)^2+30(-1)^{p+q}(9q+8)(q+1)^2)+\gamma_S(2160+4200p+5464q+3420p^2-540p^3+4800q^2+1040q^3+720q^4+216q^5+7440pq^2+10920p^2q-1440pq^3-720pq^4+12600p^2q^2+2160p^2q^3+1080p^3q^2+9000pq+60(-1)^p(9q+8)(q+1)(q+2)+60(-1)^q(9p+8)(p+1)(p+2)+60(-1)^{p+q}(9q+8)(q+1)(q+2))\}$.

14. $w^+Mo_e(P_T(p,q)) = \frac{1}{5}\rho_{MS}^3\{860p+1032q+2880pq+2700pq^2+3420p^2q-360pq^3-360pq^4+600p^2-270p^3+860q^2+60q^3+180q^4+108q^5+4680p^2q^2+1080p^2q^3+540p^3q^2+330+30(-1)^p(9q+8)(q+1)^2+30(-1)^q(9p+8)(p+1)^2+30(-1)^{p+q}(9q+8)(q+1)^2\}$.

15. $w^+Mo_t(P_T(p,q)) = \frac{1}{30}\rho_{MS}^2\{\rho_{MS}(1980+5160p+6192q+3600p^2-1620p^3+5160q^2+360q^3+1080q^4+648q^5+16200pq^2+20520p^2q-2160pq^3-2160pq^4+28080p^2q^2+6480p^2q^3+3240p^3q^2+17280pq+180(-1)^p(9q+8)(q+1)^2+180(-1)^q(9p+8)(p+1)^2+180(-1)^{p+q}(9q+8)(q+1)^2)+\gamma_M(540+930p+1392q+600p^2-270p^3+1200q^2+180q^3+180q^4+108q^5+2880pq+2700pq^2+3420p^2q-360pq^3-360pq^4+4680p^2q^2+1080p^2q^3+540p^3q^2+30(-1)^p(9q+8)(q+1)^2+30(-1)^q(9p+8)(p+1)^2+30(-1)^{p+q}(9q+8)(q+1)^2)+\gamma_S(2160+4200p+5464q+3420p^2-540p^3+4800q^2+1040q^3+720q^4+216q^5+7440pq^2+10920p^2q-1440pq^3-720pq^4+12600p^2q^2+2160p^2q^3+1080p^3q^2+9000pq+60(-1)^p(9q+8)(q+1)(q+2)+60(-1)^q(9p+8)(p+1)(p+2)+60(-1)^{p+q}(9q+8)(q+1)(q+2))\}$.

16. $w^*Mo(P_T(p,q)) = \frac{1}{5}\rho_{MS}^3\{\gamma_M(30p+144q+60p^2-90p^3+240q^2+60q^3+60q^4+36q^5+660pq^2+900p^2q-120pq^3-120pq^4+1440p^2q^2+360p^2q^3+180p^3q^2+480pq+30(-1)^p(3q+2)(q+1)^2+30(-1)^q(3p+2)(p+1)^2+30(-1)^{p+q}(3q+2)(q+1)^2)+\gamma_S(240p+568q+540p^2-180p^3+960q^2+320q^3+240q^4+72q^5+1920pq^2+3000p^2q-480pq^3-240pq^4+3960p^2q^2+720p^2q^3+360p^3q^2+1560pq+60(-1)^p(3q+2)(q+1)(q+2)+60(-1)^q(3p+2)(p+1)(p+2)+60(-1)^{p+q}(3q+2)(q+1)(q+2))\}$.

17. $w^*Mo_e(P_T(p,q)) = \frac{6}{5}\rho_{MS}^4\{20p+64q+480pq+660pq^2+900p^2q-120pq^3-120pq^4+60p^2-90p^3+140q^2+20q^3+60q^4+36q^5+1440p^2q^2+360p^2q^3+180p^3q^2-30+30(-1)^p(3q+2)(q+1)^2+30(-1)^q(3p+2)(p+1)^2+30(-1)^{p+q}(3q+2)(q+1)^2\}$.

18. $w^*Mo_t(P_T(p,q)) = \frac{1}{5}\rho_{MS}^3\{\rho_{MS}(120p-180+384q+360p^2-540p^3+840q^2+120q^3+360q^4+216q^5+3960pq^2+5400p^2q-720pq^3-720pq^4+2160p^2q^3+1080p^3q^2+8640p^2q^2+2880pq+180(-1)^p(3q+2)(q+1)^2+180(-1)^q(3p+2)(p+1)^2+180(-1)^{p+q}(3q+2)(q+1)^2)+\gamma_M(30p+144q+60p^2-$

$90p^3 + 240q^2 + 60q^3 + 60q^4 + 36q^5 + 660pq^2 + 900p^2q - 120pq^3 - 120pq^4 + 1440p^2q^2 + 360p^2q^3 + 180p^3q^2 + 480pq + 30(-1)^p(3q+2)(q+1)^2 + 30(-1)^q(3p+2)(p+1)^2 + 30(-1)^{p+q}(3q+2)(q+1)^2) + \gamma_S(240p + 568q + 540p^2 - 180p^3 + 960q^2 + 320q^3 + 240q^4 + 72q^5 + 1920pq^2 + 3000p^2q - 480pq^3 - 240pq^4 + 3960p^2q^2 + 720p^2q^3 + 360p^3q^2 + 1560pq + 60(-1)^p(3q+2)(q+1)(q+2) + 60(-1)^q(3p+2)(p+1)(p+2) + 60(-1)^{p+q}(3q+2)(q+1)(q+2))\}$.

Proof. We have $|V_\gamma(P_T(p,q))| = \gamma_M(p+1)(q+1) + \gamma_S(6+4p+4q+2pq)$ and $|E_\rho(P_T(p,q))| = 6\rho_{MS}(p+1)(q+1)$ with the total number of vertices and edges as $5p+5q+3pq+7$ and $6(p+1)(q+1)$ respectively. The strength-weighted parameters of all the Θ-classes are tabulated in Table 5. Furthermore, $X_{2i}^{Tp}(w) = |V_\delta(BT_T(n,p,q))| - X_{1i}^{Tp}(w)$ and $X_{2i}^{Tp}(s) = |E_\zeta(BT_T(n,p,q))| - X_{1i}^{Tp}(s) - X_{3i}^{Tp}(s)$.

Table 5: Strength-weighted parameters of $P_T(p,q)/X_{ki}^{Tp}$, $X \in \{H, O, A, P\}$

Θ-class	Vertex parameters (w_v, s_v)	Edge parameters ($w_e^*/w_e^+, s_e$)
H_i^{Tp}:$1 \le i \le q$	$H_{1i}^{Tp}(w) = \gamma_S(1+4i+p+2ip)$	$H_{3i}^{Tp}(s) = 2\rho_{MS}(p+1)$
	$+i\gamma_M(p+1)$	$H_{3i}^{Tp}(w^+) = 2\rho_{MS}(9p+8)$
	$H_{1i}^{Tp}(s) = \rho_{MS}(6i-1)(p+1)$	$H_{3i}^{Tp}(w^*) = 12\rho_{MS}^2(3p+2)$
O_i^{Tp}:$1 \le i \le p$	$O_{1i}^{Tp}(w) = \gamma_S(1+4i+q+2iq)$	$O_{3i}^{Tp}(s) = 2\rho_{MS}(q+1)$
	$+i\gamma_M(q+1)$	$O_{3i}^{Tp}(w^+) = 2\rho_{MS}(9q+8)$
	$O_{1i}^{Tp}(s) = \rho_{MS}(6i-1)(q+1)$	$O_{3i}^{Tp}(w^*) = 12\rho_{MS}^2(3q+2)$
A_i^{Tp}:$1 \le i \le q$	$A_{1i}^{Tp}(w) = \gamma_S(1+3i+i^2)$	$A_{3i}^{Tp}(s) = \rho_{MS}(2i+1)$
	$+i\gamma_M(i+1)/2$	$A_{3i}^{Tp}(w^+) = \rho_{MS}(18i+7)$
	$A_{1i}^{Tp}(s) = i\rho_{MS}(3i+2)$	$A_{3i}^{Tp}(w^*) = 6\rho_{MS}^2(6i+1)$
A_i^{Tp}:$q+1 \le i \le p$	$A_{1i}^{Tp}(w) = (\gamma_S(2+8i-2q-2q^2+4iq)$	$A_{3i}^{Tp}(s) = 2\rho_{MS}(q+1)$
	$+\gamma_M(2i-q-q^2+2iq))/2$	$A_{3i}^{Tp}(w^+) = 2\rho_{MS}(9q+8)$
	$A_{1i}^{Tp}(s) = \rho_{MS}(q+1)(6i-3q-1)$	$A_{3i}^{Tp}(w^*) = 12\rho_{MS}^2(3q+2)$
A_{-i}^{Tp}:$1 \le i \le q$	$A_{-1i}^{Tp}(w) = (i+1)((i+2)\gamma_S+$	$A_{-3i}^{Tp}(s) = \rho_{MS}(i+1)$
	$i\gamma_M)/2$	$A_{-3i}^{Tp}(w^+) = \rho_{MS}(6i+4)$
	$A_{-1i}^{Tp}(s) = 3i\rho_{MS}(i+1)/2$	$A_{-3i}^{Tp}(w^*) = \rho_{MS}(9i+3)$
$P_i^{Tp} : 1 \le i \le 2(p+q+3)$	$P_{1i}^{Tp}(w) = \gamma_S$	$P_{3i}^{Tp}(s) = \rho_{MS}$
		$P_{3i}^{Tp}(w^+) = 7\rho_{MS}$
	$P_{1i}^{Tp}(s) = 0$	$P_{3i}^{Tp}(w^*) = 6\rho_{MS}^2$

We therefore derive the indices $TI \in \{W, W_e, W_{ve}, Sz_v, Sz_e, Sz_{ev}, PI, S, Gut, Mo, Mo_e, Mo_t, w^+Mo, w^+Mo_e, w^+Mo_t, w^*Mo, w^*Mo_e, w^*Mo_t\}$ using the expression,

$$TI(P_T(p,q)) = \sum_{i=1}^{q} TI(P_T(p,q)/H_i^{Tp}) + \sum_{i=1}^{p} TI(P_T(p,q)/O_i^{Tp}) + 2\sum_{i=1}^{q} TI(P_T(p,q)/A_i^{Tp}) + \\ + \sum_{i=q+1}^{p} TI(P_T(p,q)/A_i^{Tp}) + \sum_{i=1}^{2(p+q+3)} TI(P_T(p,q)/P_i^{Tp}).$$

□